NASA SP-114

# SPACE TECHNOLOGY

Volume VI

## SPACE SCIENCES

T. A. Farley
*University of California, Los Angeles*

*Scientific and Technical Information Division* 1966
NATIONAL AERONAUTICS AND SPACE ADMINISTRATION
*Washington, D.C.*

FOR SALE BY THE SUPERINTENDENT OF DOCUMENTS, U.S. GOVERNMENT
PRINTING OFFICE, WASHINGTON, D.C., 20402 - PRICE 35 CENTS

# Foreword

THIS IS ONE of a series of publications derived from the interdisciplinary Institutes in Space Science and Technology sponsored by the National Aeronautics and Space Administration. The concept underlying these Institutes has been to acquaint and interest outstanding undergraduates in the rapidly developing technology created by the exploration of space. The program has been built around a core of lectures and discussions on space-related activities. The development of this resource material represents another part of the tangible output resulting from the nation's space program. NASA will continue to encourage and stimulate the development of such a body of knowledge, for this represents a contribution and a commitment to the education of tomorrow's scientific and technical leaders.

This volume was developed from lecture notes used in a course in space sciences given in the summer of 1965 at the University of California at Los Angeles (UCLA) under the joint sponsorship of the California Universities' Council on Space Sciences and NASA. Other volumes in the series originated from courses presented at the California Institute of Technology (Caltech) and taught by staff members from Caltech, the Jet Propulsion Laboratory, and industry.

JOHN T. HOLLOWAY, *Acting Director*
*Office of Grants and Research Contracts*
*Office of Space Science and Applications*

*July 1966*

# Contents

CHAPTER 1

# The Geomagnetic Field

## THE NEAR GEOMAGNETIC FIELD

### The Steady Component

FOR MANY CENTURIES the magnetic field of the Earth has been known and used in navigation. For the last 50 years the field and its time variations have been studied intensively. A large body of data and the terminology to interpret it was therefore in existence long before it became possible to make measurements on rocket and satellite vehicles. In spite of this very considerable effort, neither the origin of the main field nor the origin of its main variations is known in great detail.

The magnetic field, $B$, of the Earth is a vector quantity, and a complete measurement of the field at a point must specify the direction and magnitude. The physical quantity which is denoted by $B$ is magnetic induction. It is this quantity which is of most interest in a description of the geomagnetic field because the magnetic induction determines the behavior of charged particles in the field. The symbol $H$ is commonly used for another physical quantity called magnetic field intensity. In some of the older literature the symbol $H$ is used for magnetic induction, and this is a possible source of confusion. The units of magnetic induction in the cgs system are the gauss and its submultiple the gamma ($=10^{-5}$ gauss). The mks unit of magnetic induction is the weber/meter$^2$ ($=10^4$ gauss).

The vector $B$ may be specified by any three of the following measurements, all in common use for Earth-surface measurements. If the magnitude of the field is known, any two will suffice.

- $X$ Northward (geographic) component
- $Y$ Eastward component
- $Z$ Downward vertical component
- $H$ Horizontal component
- $I$ Inclination (dip): Angle between the horizontal and total field vector

*D* Declination: Angle measured eastward between true and magnetic north; i.e., between $X$ and $H$

Measurements on the surface of the Earth have demonstrated that the magnetic field of the Earth, at points on or above the Earth's surface, is roughly that of a dipole. This is the same field as that of a bar magnet when one is not too close to the magnet. The field lines of a dipole are illustrated in figure 1.1.

The vector field of a dipole at any point may be found by taking derivatives in spherical coordinates of the scalar potential of a dipole:

$$V = -\frac{M \cos \theta}{r^2}$$

$$\mathbf{B} = -\nabla \mathbf{V}$$

so that the magnitudes of the components are

$$Z = \frac{2M \cos \theta}{r^3}$$

$$H = \frac{M \sin \theta}{r^3}$$

where $V$ is the magnetic scalar potential, $\theta$ is the geographic colatitude, $r$ is the distance from the origin, and $M$ is the magnetic moment of the dipole. (The value of $M$ is $8.06 \times 10^{25}$ gauss-cm$^3$ for the Earth.)

The equation of a field line is

$$r = r_0 \sin^2 \theta$$

where $r_0$ is the distance from the dipole origin at which the line crosses the magnetic equator. The variation of the magnitude of the field along a field line is

$$\frac{B}{B_0} = \frac{(4 - 3 \cos^2 \lambda)^{1/2}}{\cos^6 \lambda}$$

where $B_0$ is the magnitude of the field at the equator, and $\lambda$ is the magnetic latitude (rather than the colatitude $\theta$, used above).

A reasonable fit to the Earth's surface field may be obtained by placing the dipole at the center of the Earth and orienting it so that the magnetic pole of the Earth in the Northern Hemisphere is located at 78.5° N geographic latitude and 291° E geographic longitude. (This pole is actually a *south* magnetic pole by the usual convention, since field lines converge at this point, while diverging from the opposite pole in the Southern Hemisphere.) With this fit the magnetic latitude and longitude of any point on or above the surface of the Earth may be found from a simple rotation of the geographic coordinates. It has been found, as might have been expected, that many geophysical phenomena which are dependent on the geomagnetic field are symmetric in magnetic coordinates, but not in geographic coordinates.

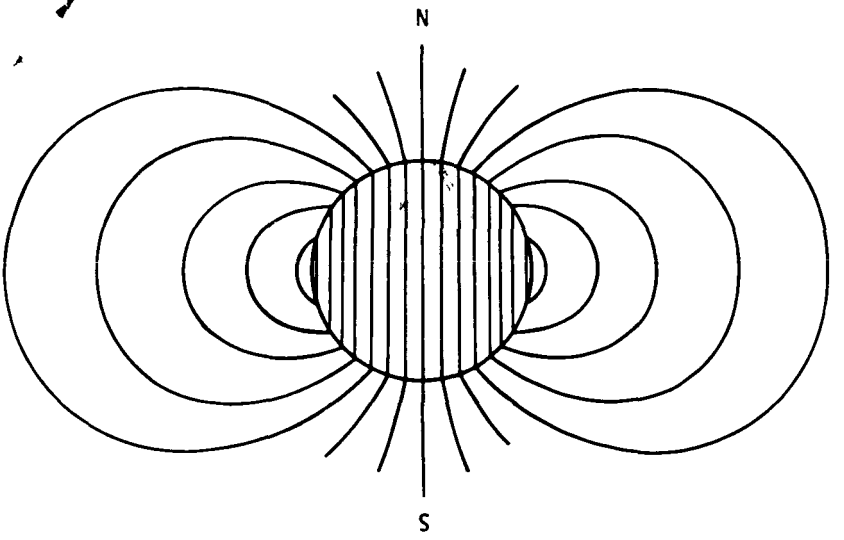


FIGURE 1.1—Lines of induction of a magnetic dipole (ref. 1).

A somewhat better fit may be obtained by displacing the dipole 340 kilometers from the center of the Earth along a line with coordinates 6.5° N and 161.8° E. Such a dipole offers an inconvenient origin for the definition of a magnetic coordinate system, and it is rarely used. When a better description of the field than the Earth-centered dipole is desired, a spherical harmonic expansion of the magnetic scalar potential is used.

Such an expansion is a convergent infinite series in a spherical coordinate system whose origin is located at the center of the Earth and whose polar axis is in the direction of the geographic North Pole. The expansion may be written

$$V = \sum_{n=0}^{\infty} \left(\frac{a}{r}\right)^{n+1} \sum_{m=0}^{\infty} P_n^m (\cos \theta) \ (g_n^m \cos m\Psi + h_n^m \sin m\Psi)$$

where $a$ is the radius of the Earth, $\Psi$ is the east longitude, $P_n^m (\cos \theta)$ is the normalized associated Legendre polynomial of degree $n$ and order $m$, and $g_n^m$ and $h_n^m$ are Gaussian coefficients to be determined by actual measurements of the field. This representation is used because it is known that the series must converge, and because it is known that the field expressed in this way will be consistent with Maxwell's equations. These expressions are true only for regions of space in which there are no currents and therefore cannot be used within the Earth because of the internal source currents for the geomagnetic field. The fact that the field external to the Earth can be successfully represented in this way is taken as proof that external currents can contribute at most only one part in a thousand to the Earth-surface field.

The magnitude and direction of the magnetic induction $B$ is computed as before by taking the gradient of the scalar potential.

Various sets of coefficients have been determined by fitting the data. Some sets have contained as many as 512 coefficients. The coefficients must be updated from time to time, since there are slow secular variations of internal origin. The magnetic moment of the Earth appears to have decreased about 5 percent in the last century. While the exact origin of the Earth's field is not known, it is thought to arise from large circulating currents within the Earth. The currents are believed to be driven by the rotation of the Earth, perhaps because of differential rotation between the liquid core and the solid mantle. This theory predicts that planets which rotate very slowly or not at all (Venus, for example) will have no magnetic field. Space-probe experiments will probably be able to test this theory in considerable detail.

#### The Variable Component

Day-to-day observations of the Earth-surface geomagnetic field over many years have permitted detailed analysis of certain time variations without revealing very clearly their origins. The very slow variations of internal origin have been mapped over the entire Earth to obtain some information about the changing current system within the Earth. Another type of variation with a period of 1 solar day has been discovered. During what are called magnetically quiet periods, the variation is smooth and regular. A typical example is shown in figure 1.2. This diurnal variation is called $S_q$ or solar quiet variation. On what are termed magnetically noisy days, the $S_q$ variation may be enhanced or obscured entirely. The enhanced $S_q$ variation is called $S_D$ (disturbance daily variation). An additional lunar daily variation $L$ of small amplitude is superimposed on $S_q$. All these variations depend on the geomagnetic latitude, the season, and on the phase of the 11-year solar cycle.

Correlation of the observations indicates that large-scale current systems exist as thin sheets in the ionosphere at altitudes between 100

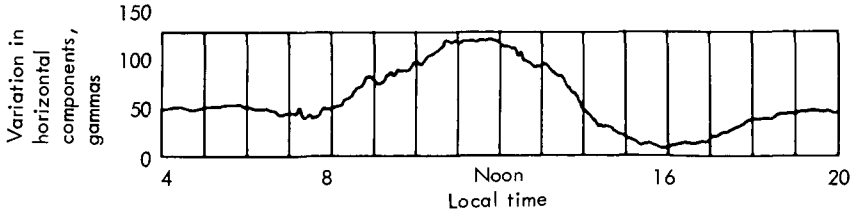


**FIGURE 1.2—Magnetic variometer record showing $S_q+L$ variation in the horizontal component at the magnetic dip equator (ref. 1).**

and 150 kilometers. The currents are thought to be driven by the daily heating and cooling effect of the Sun, which transports ions and electrons across field lines. This produces a transverse force which drives the current. A current system in the ionosphere which could produce the $S_q$ variation is shown in figure 1.3. Various secondary current systems are invoked to account for observations in the polar regions. Seasonal and other time-dependent changes in the conductivity and wind motions of the ionosphere may correspond to observed changes in the $S_q$ variation.

The complicated time-dependent structure of the ionosphere may be studied with rocket-borne magnetometers, ionization probes, mass spectrometers, electric field meters, and special thermometers. Sodium vapor or other chemicals are released to study wind motions. Observations of these phenomena have just begun and a period of rapid scien-

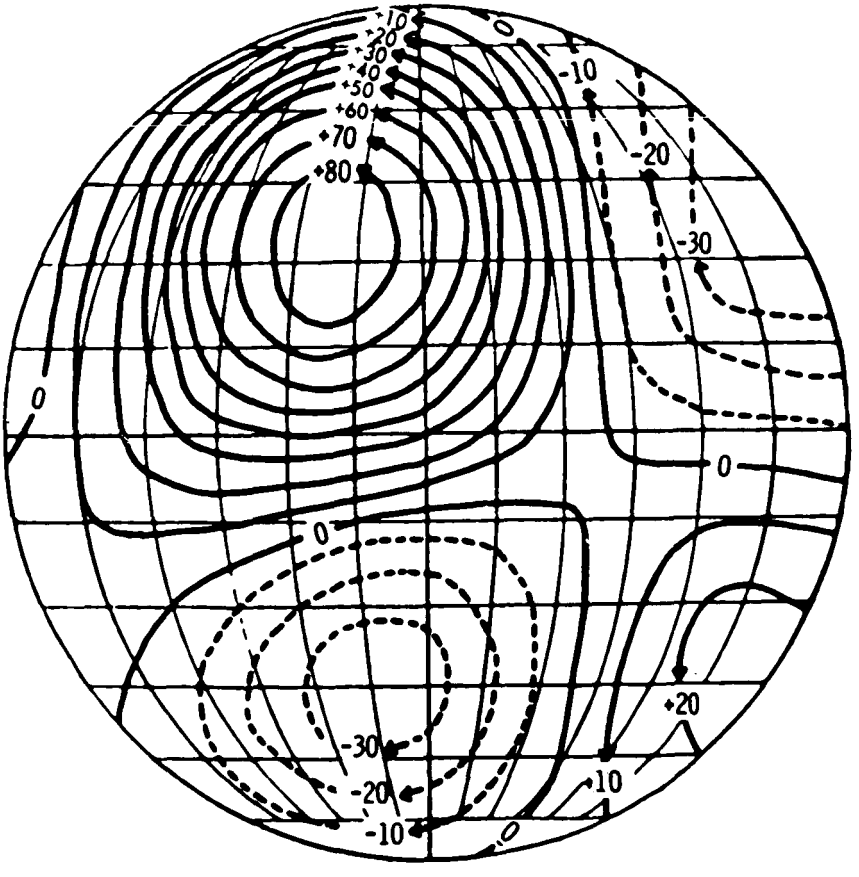


**FIGURE 1.3—A current system which could produce the $S_q$ variation during the northern summer. Ten thousand amperes flow between each current contour (ref. 1).**

tific progress is just ahead. It is unfortunate that this very interesting region has an atmospheric density too great to permit a satellite to have an appreciable lifetime, so that the experiments must be performed on sounding rockets whose flights are of short duration.

## THE DISTANT GEOMAGNETIC FIELD

### The Ring Current

In addition to the magnetic-field variations thought to be caused by ionospheric currents, characteristic variations of the kind found in figure 1.4 are seen. The figure shows the variation in the horizontal component, measured at the Earth's surface. The occurrence of this particular variation is usually, but not always, preceded by a solar flare. A solar flare is a disturbance on the Sun in which large numbers of charged particles are ejected in a cloud which may eventually envelop the Earth, producing the observed magnetic-field variation.

The short positive deviation of the field shown in figure 1.4 is called the initial phase. It is probably the result of a compression of the entire field by the charged-particle cloud as it envelops the Earth. The effect is transmitted to the Earth's surface as a hydromagnetic

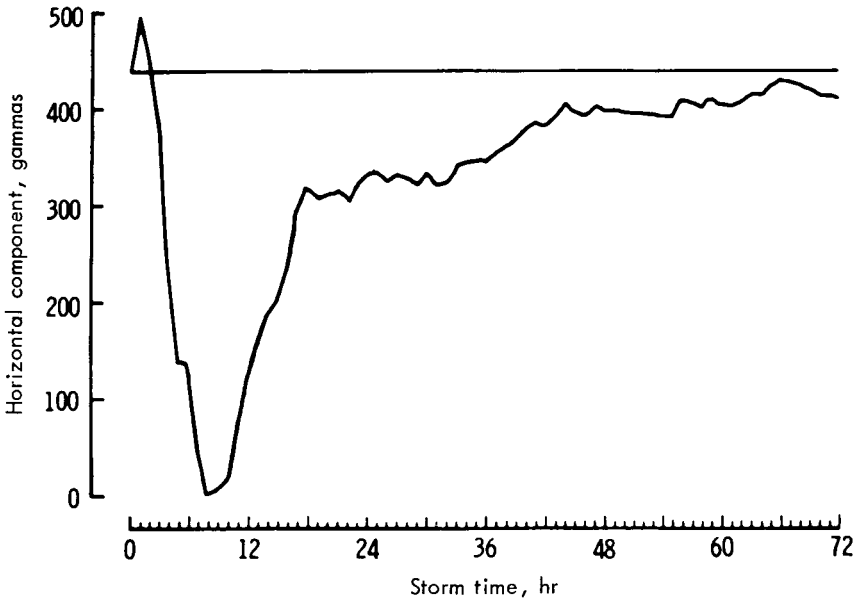


**FIGURE 1.4—The horizontal component of the Earth's field during a typical large geomagnetic storm. The positive initial phase, the negative main phase, and the slow recovery are shown (ref. 1).**

wave so that it appears almost simultaneously over the entire surface of the Earth.

The deep negative deviation is believed due to a westward-flowing ring current around the Earth. This period of the magnetic storm is called the main phase. The slow return to normal field magnitude is called the recovery phase. It is due to a gradual decay of the ring current set up by the storm. The extraterrestrial ring current was originally proposed more than 50 years ago as the simplest model which could account for the main-phase depression of the horizontal component. No detailed model of such a current appeared until Singer in 1957 proposed that it consisted of large numbers of charged particles trapped and drifting in the geomagnetic field. The model has since undergone detailed calculations by a number of investigators.

Satellites have provided an opportunity to investigate the proposed ring current, and a number of satellite magnetometer experiments were specifically designed to search for it. Nonetheless, confirmation of the theory has been difficult, and a completely satisfactory experimental picture has not yet emerged. The ring current has been variously reported at geocentric distances ranging from 3.5 Earth radii (Lunik I) to 10 Earth radii (Explorer VI), and some investigators have not seen it at all. Some of the problems have involved the instruments. Many of the measurements have not determined the total vector field, but have measured only one component or just the magnitude. The expected deviation from the normal field is small at the actual position of the current, especially if the current is at 4 Earth radii or less. Small errors in measurement of the spacecraft position and orientation can mask the deviation. Figure 1.5 shows the magnetic-field measurements made by Cahill on Explorer XIV on January 7, 1963. A comparison is made in the figure with the field predicted by the spherical harmonic expansion. A persistent depression below the predicted field is apparent, but the possibility remains that this is caused by calibration drift or errors in the orbit determination.

The ring current has proved so elusive that an alternative model has been proposed. In this model the ring current is not composed of charged particles drifting in the magnetic field, but is instead the surface currents which flow at the boundary or interface between the geomagnetic field and the tenuous plasma which fills interplanetary space. Recent theoretical work on the boundary-surface currents indicates that they are probably too small to account for the Earth-surface observations.

It might be supposed that the ring current could more easily be detected by searching for the particles which compose it rather than for the magnetic field which accompanies it. Unfortunately, the region of space from 1 to 10 Earth radii contains high fluxes of very energetic

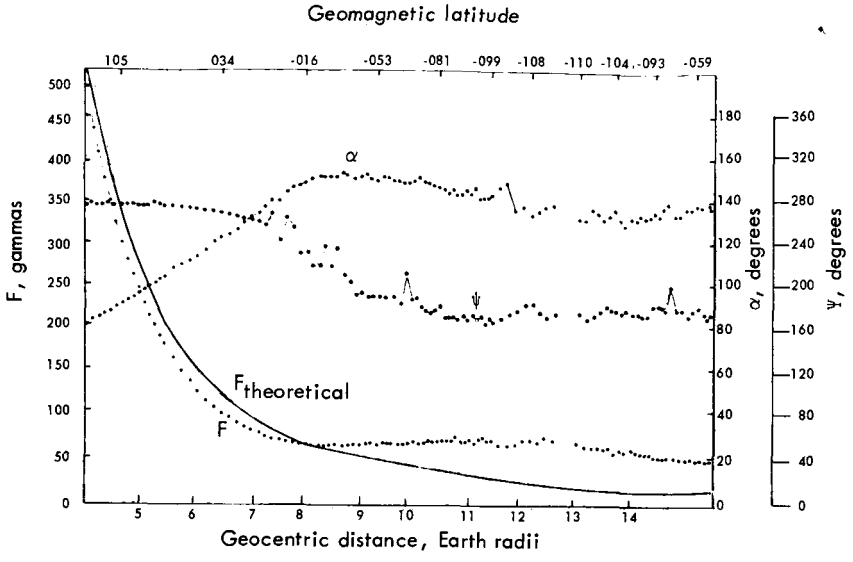


**FIGURE 1.5—A magnetometer record from the Explorer XIV satellite. The field direction is given by $\alpha$ and $\psi$. The observed magnitude F is compared with the magnitude $F_{theoretical}$ computed from the spherical harmonic expansion (reference field) (ref. 1).**

trapped particles. These trapped particles certainly do constitute a ring current according to the theory of their drift motion. Their density, however, is too small to account for more than an insignificant fraction of the ring current. These energetic particles can seriously affect a detector designed to search for ring-current particles.

The ring current, if it exists, must consist of much larger number densities of particles which have energies below the threshold of most of the charged-particle detectors which have been employed. Recent experiments have demonstrated the presence of protons in the energy range from 100 keV to 4.5 MeV whose number densities are large enough to produce significant magnetic effects. The observed enhancement of these protons during a magnetic storm is inadequate to produce the decrease in field noted at ground observatories. It seems likely, however, that the observed protons constitute the high-energy portion of a distribution which extends down to perhaps 1 keV. The lower energy protons, as yet undetected, may constitute a sufficiently large current to account for the observations.

Hoffman and Bracken have computed the electric current of the observed protons during a magnetically quiet period using the guiding-center approximation for the individual particle motions. They find a total current of 0.59 million amperes, having a magnetic moment 2.9 percent of that of the Earth. The disturbance field (i.e., the field

caused by this current) is shown in figure 1.6. This field would reduce the Earth-surface field by only 9 gammas at the magnetic equator, and might escape detection entirely. Nevertheless, it is reasonable to assume that the field of a larger number density of lower energy protons would be similar in direction and larger in magnitude, producing the typical 500-gamma decrease illustrated in figure 1.4 for a magnetic storm period.

The recovery phase of a magnetic storm is probably due to the gradual decay of the ring current over a period of several days. If the storm-time ring current is indeed composed of protons in the energy range from 1 to 100 keV, the observed decay over several days is consistent with the lifetimes of the protons. The trapping lifetimes of these particles are determined principally by charge exchange with neutral hydrogen atoms of thermal energies and by Coulomb collisions with other charged particles. The origin of these particles at the onset of a magnetic storm is speculative. A possible origin is discussed in chapter 2 on the Van Allen radiation belt.

It is unlikely that electrons contribute significantly to the ring current, because the current produced by trapped particles is proportional to their momenta. Particles of equal kinetic energy have momenta which are proportional to the square root of their masses. Electrons of the same kinetic energy produce a much smaller effect than do

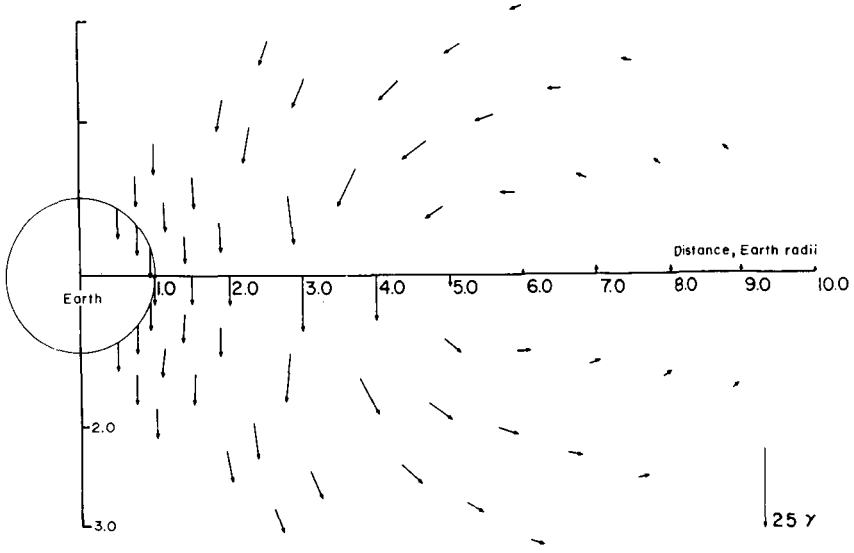


**FIGURE 1.6—Vector magnetic field on a meridian plane caused by the proton ring current (ref. 2).**

protons, and sufficient electrons to produce a significant ring current have not been found at any energy.

The calculation of the magnetic field caused by the motion of particles trapped in the field presents theoretical difficulties. The drift motions, upon which the current depends, are readily calculated using the guiding-center approximation, once the field has been specified. If the particles materially alter the field, as they do during a geomagnetic storm, the field cannot be specified in advance and the current cannot be computed. The usual approach to this problem is a two-step solution in which the perturbation fields are first ignored in order to compute the current and the perturbation field. In the second step the perturbation fields found in the first step are added to the geomagnetic field, and the current and perturbation fields are recomputed. If the perturbation fields are not too large in relation to the geomagnetic field, the process will converge rapidly. Even a two-step problem, however, is mathematically complex.

#### The Magnetopause

If the interplanetary space were a perfect vacuum, the geomagnetic field would extend to infinity. There is adequate evidence that interplanetary space is not empty, but filled with a neutral ionized gas. Recognition of this problem dates back to 1931, when Chapman and Ferraro, in a series of papers covering many years, proposed that streams of ionized gas from the Sun were incident on the geomagnetic field, causing a number of observable effects. It was quickly recognized that this plasma stream constituted a diamagnetic gas of high conductivity which would tend to exclude any external field. The mechanism is a simple application of Lenz's law: The particles on the plasma boundary will take up ordered motions creating a magnetic field which just cancels the external field at all points in the plasma.

The application of this idea to the geomagnetic field indicated that the field would be confined to a cavity, along the surface of which currents flow, resulting in a net field of zero at all points external to the cavity.

Determining the boundary-surface shape became known as the Chapman-Ferraro problem. In idealized form the problem consists of a cold, ionized, electrically neutral plasma incident at right angles to a magnetic dipole. The particles are assumed to act independently of one another, and collisions and collective motions are ignored.

Since the incident ions have greater momenta than the electrons, they will penetrate more deeply into the field than the electrons. This charge separation constitutes an electric field perpendicular to the boundary. The electric field accelerates the electrons at the ex-

pense of the ion kinetic energy. The ions are therefore reflected primarily by the electric field, and the electrons by the magnetic field. Calculations have demonstrated that the boundary under these conditions will be only about 1 kilometer thick.

It is possible that any such electric field would be shorted by currents along field lines which connect to that great reservoir of charge, the ionosphere. If this is the case, the boundary thickness will be determined by the ion cyclotron radii, and may be approximately 10 kilometers thick, which is still quite thin compared with the radius of curvature of the surface.

With or without an electric field, it follows readily from symmetry considerations that the particle exit path from the boundary must be the mirror image of its incident path. We have, then, specular reflection—the angle of incidence of the particle is equal to the angle of reflection.

Once we have been assured that the boundary is thin and that specular reflection occurs, no further details of the particle motions are necessary to determine the shape of the boundary. The shape is determined by Maxwell's equations and the two boundary conditions. The first boundary condition is that the normal component of $B$ be continuous. Since $B$ is zero everywhere outside, the normal component of $B$ must be zero inside. The second boundary condition is that the pressure exerted at the boundary by the tangential component of $B$ must be balanced by the particle pressure exerted from outside the boundary. The particle pressure is readily computed from the particle number density and the stream velocity if specular reflection occurs.

Unfortunately the solution for the boundary surface requires that the field at the boundary be known. The field cannot be determined until the surface currents are known, and the surface currents cannot be determined unless the boundary is known.

Various approximations have been used to obtain some idea of the surface. One such approximation involves an image dipole placed at twice the distance from the first dipole to the boundary. This simulates the plasma-stream pressure on the dipole, but it is a rather poor approximation to the real problem. The two-dimensional problem in the meridian plane containing the dipole and dipole-Sun line has been solved exactly, providing considerable insight into the three-dimensional problem.

Beard suggested that a self-consistent technique of successive approximations be employed. As a start, it is assumed that the field just inside the boundary is double the dipole value, since this would actually be the case for a uniform field bounded by a plane current sheet. The boundary is computed using this assumption, and the sur-

face currents are computed. A second approximation for the field at the boundary is computed from the surface currents using the Biot-Savart law and the process is repeated. The successive solutions are tested by computing the external field, which should, of course, be zero. The method converges rapidly, and the fourth approximation

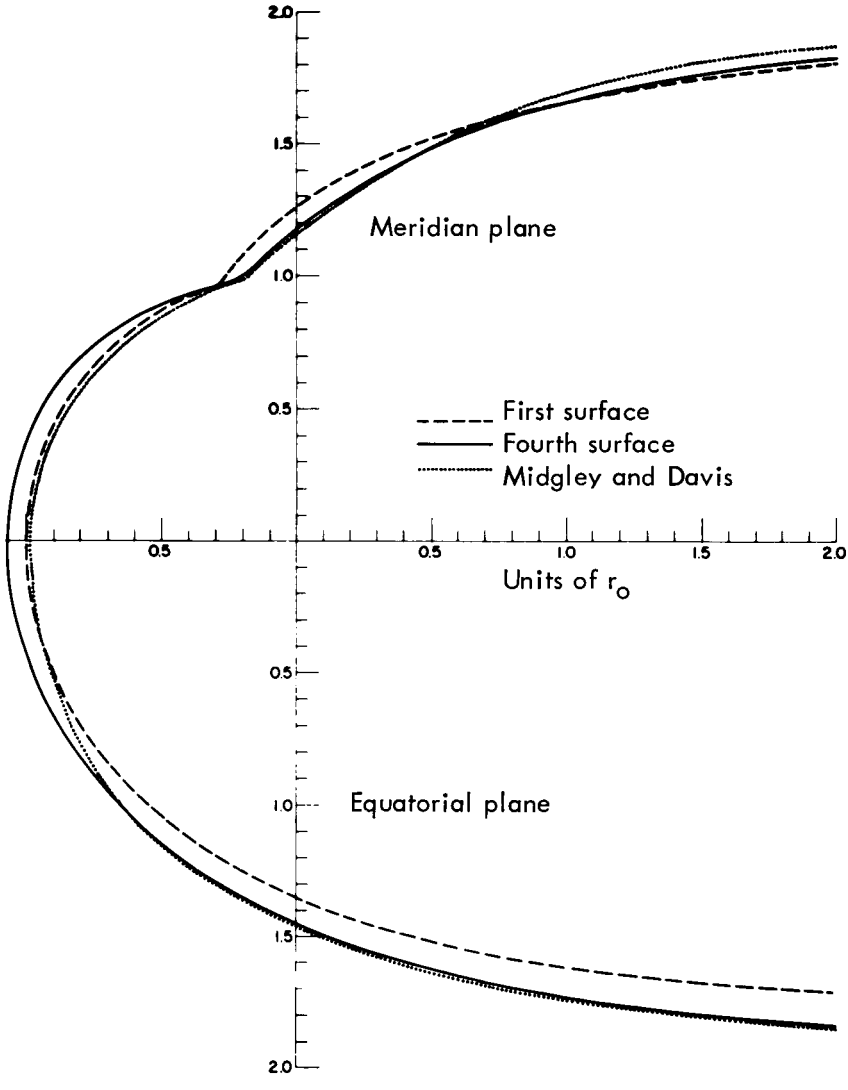


**FIGURE 1.7—Computed shape of the magnetospheric boundary. A section through a meridian plane is shown above the horizontal axis, and a section through the equatorial plane below the axis (ref. 3).**

surface has external fields as small as the errors in the numerical integrations.

Figure 1.7 shows the boundary surface in two planes cut through the dipole. The curve above the horizontal axis is the solution in the meridian plane above the equator of the dipole. The curve below the horizontal axis is the solution in the equatorial plane of the dipole. The solar wind is incident from the left. The distance is measured in units of $r_0$, the distance to the boundary along the Earth-Sun line in the first approximation surface. Note that the surface does not close on the night side of the magnetosphere because this model assumes a cold plasma streaming from the Sun with no transverse velocity component. There is therefore no pressure exerted on the surface in a direction perpendicular to the Earth-Sun line.

Mead has computed the total field at points within the magnetosphere including the component due to the geomagnetic field and the component due to the surface currents. The values of the field computed in this way have been used to evaluate the coefficients in a spherical harmonic expansion of the field. The expansion can then be

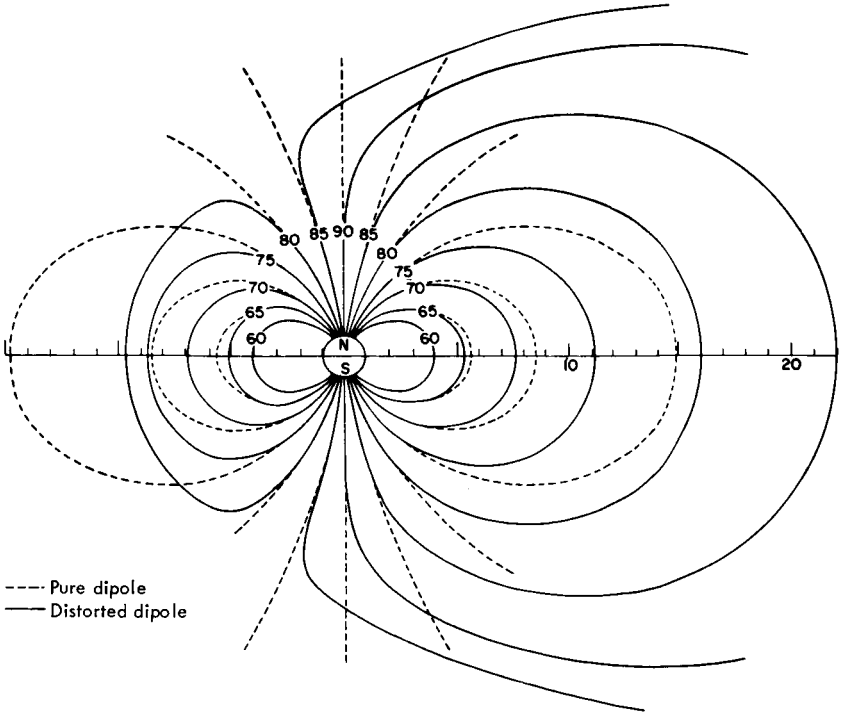


**FIGURE 1.8—Field-line configuration in the noon-midnight meridian plane. The dipole lines are compressed on both the daytime and nighttime side (ref. 4).**

used to compute the field at every point. A comparison of the dipole field and the field distorted by these surface currents is shown in figure 1.8. Once again the solar wind is incident from the left. When the distance to the boundary along the Earth-Sun line is 10 Earth radii, there exists a critical latitude of 83° above which field lines originating on the day side of the Earth are blown back to the night side. The situation creates a neutral line along which a charged particle could penetrate to the surface of the Earth at 83° north or south latitude without experiencing any magnetic force; i.e., without crossing any magnetic field lines. All field lines which leave the Earth at latitudes greater than 83° will cross the geomagnetic equator within ±75° of the midnight meridian in this model.

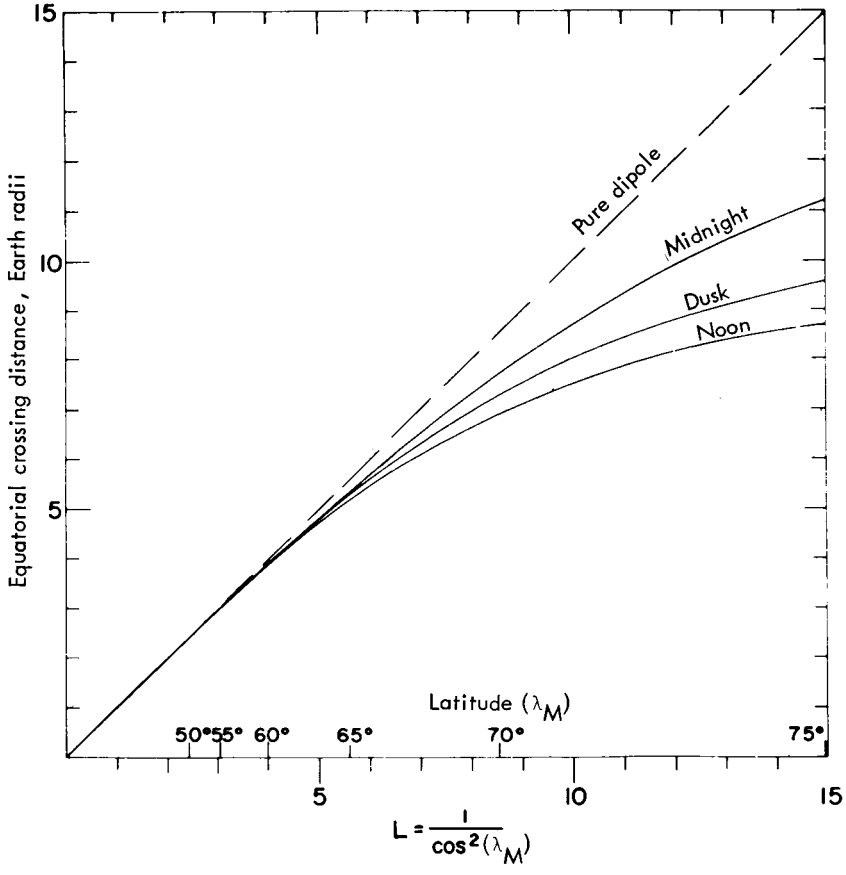


**FIGURE 1.9—Compression of the field lines at the equator for a field termination at 10 Earth radii. All field lines cross the geomagnetic equator at distances less than they would for an undistorted dipole (ref. 4).**

A careful inspection of figure 1.8 reveals an unexpected feature. The field is compressed on both the day and night sides of the Earth. That is to say, field lines which leave the Earth's surface at a given latitude cross the magnetic equator at a shorter distance on both day and night sides when the boundary surface currents are taken into account. This situation is illustrated in figure 1.9. The compression is seen to be greatest at local noon, less at dusk, and least at local midnight.

Figure 1.10 shows the scalar value of the field in the noon meridian along field lines which emerge from the Earth at several magnetic latitudes. Note that as the latitude approaches the critical value, the field no longer possesses a single minimum at the equator as do dipole field lines. Lines near this latitude develop two minima, not far from the neutral line which extends into the Earth at the critical latitude.

The solution of the Chapman-Ferraro problem is essentially complete. Some additional features are presently being included to make the problem more realistic. For example, the solution discussed here does not include the effects of the tilt of the Earth's magnetic axis with respect to the geographic axis, nor the inclination of the

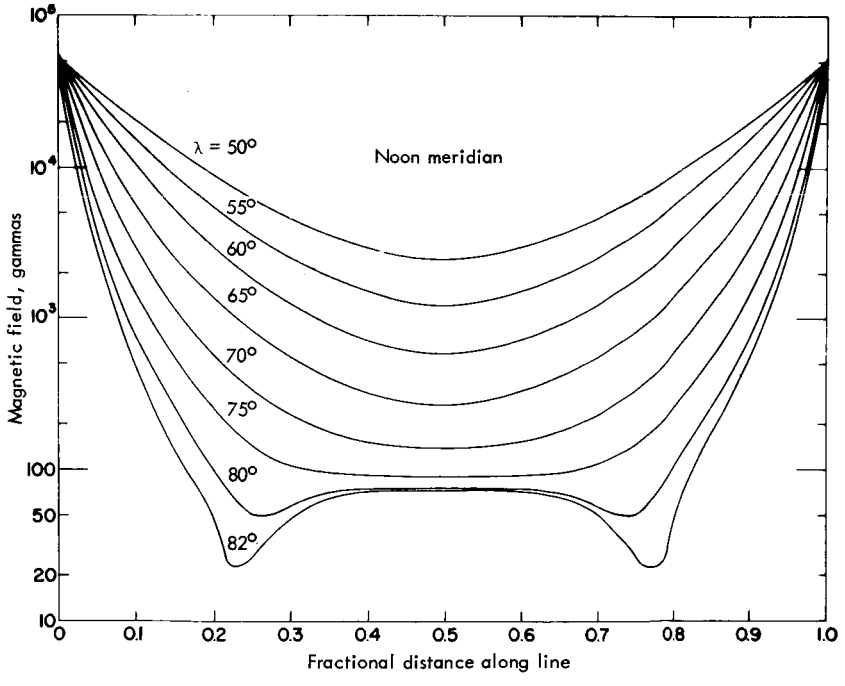


**FIGURE 1.10—Absolute magnitude of the distorted field along lines in the noon meridian (ref. 4).**

geographic axis with respect to the ecliptic plane. These two effects may add, depending on the season of the year and the time of day, so that the solar wind may at times be incident at magnetic latitudes of as much as $\pm(23.5° + 11.5°)$ instead of the 0° assumed in the model calculation. Such effects complicate the numerical solution of the problem but do not introduce any new effects.

The observations made with instruments on satellites which have traversed the boundary indicate that the model is oversimplified. The solar wind has been found to have a weak magnetic field embedded in it; the plasma is not "cold"; and significant effects are caused by the transverse components of the thermal velocities. Collective particle motions, i.e., hydromagnetic waves in the plasma, cannot be ignored. In order to see how these phenomena affect the magnetospheric boundary, it is necessary to consider the properties of the solar plasma in more detail. It will then be possible to return to the boundary and account for the experimental observations.

## MAGNETOMETERS FOR SPACE MEASUREMENTS

The magnitude of the Earth-surface magnetic induction is about 0.2 gauss (20 000 gammas). In interplanetary space, values as low as 1 gamma have been observed. A magnetometer for space research must therefore be designed to measure very small fields, but must have a dynamic range of more than four orders of magnitude if continuous measurements are to be made from the Earth's surface to interplanetary space. Three different types of magnetometers have been employed.

### The Search-Coil Magnetometer

The search-coil magnetometer is the first and simplest type and consists of a coil of wire wound on a core of high-permeability material. According to Faraday's law, a changing magnetic induction within the coil will produce an electromotive force in the coil, proportional to the rate of change of induction. This detector can measure a dc magnetic field only in a spinning spacecraft, and then it detects only the magnitude of the component perpendicular to the spin axis. It has been used on a number of spacecraft in this way. The measurements are often combined with those of a flux-gate magnetometer mounted to measure the component along the spin axis. If a Sun sensor or other orientation indicator is employed, the vector field may be computed from the search-coil and flux-gate outputs. The sensitivity of the search-coil magnetometer is increased by the high permeability

core, and by the use of a large number of turns of wire. As many as 100 000 turns have been employed.

The search coil may also be used to measure the ac component of the magnetic field from a stabilized spacecraft. Three coils may be used in a triaxial array to measure the total ac component vector. The search coil is nearly ideal for this purpose, since the sensitivity increases with increasing frequency. The increasing sensitivity helps to compensate for the decrease in spectral intensity which occurs at high frequencies in the geomagnetic field. The power at frequencies up to 1000 cps has been measured with this technique.

#### The Flux-Gate Magnetometer

The flux-gate magnetometer consists of a drive coil and a pickup coil wound on the same core. The core is of high-permeability material which saturates at a relatively low flux density. In operation a sinusoidal current in the drive coil causes the core to be driven around its nonlinear $B$–$H$ curve. The pickup coil responds to the changing magnetic induction $B$ in the core. Because of the nonlinearity of the $B$–$H$ loop in a material which saturates at low values of $H$, the pickup coil current contains the fundamental frequency of the drive coil and its harmonics. In the absence of an ambient dc field, the $B$–$H$ curve traced out is symmetrical, and odd harmonics are missing. The addition of an ambient field produces odd harmonics whose amplitude depends on the ambient-field magnitude. The odd-harmonic content is monitored as a measure of the ambient field. A single flux gate measures only the field component parallel to the core axis, and a triaxial array of detectors is necessary to measure the vector field.

Flux-gate magnetometers have been built with sensitivities as high as 0.1 gamma and they can, of course, be used on stabilized spacecraft. They are relatively simple and dependable, compared with the optical devices described below. They have to be calibrated in known fields, since they do not provide absolute measurements. Residual permanent magnetism in the core material can cause an undesirable zero offset. The construction of flux-gate probes demands a considerable amount of experience, since the characteristics of highly permeable materials are not well understood in very low fields.

#### Resonance Magnetometers

The rubidium-vapor magnetometer is an example of an instrument which provides an absolute field measurement. The output is a frequency which depends only on the magnitude of the field and several well-known atomic constants.

The instrument consists of a rubidium-vapor lamp excited by an rf field to produce the characteristic line spectra of rubidium. A particular line is selected by a filter. This light is circularly polarized, passed through an absorption cell containing rubidium vapor, and focused on an optical detector. When a magnetic field is present, the spin axis of each rubidium atom in the absorption cell precesses around the direction of the magnetic field with a characteristic frequency proportional to the magnetic induction. This characteristic frequency is called the Larmor frequency.

Under these conditions the absorption cell containing the precessing rubidium atoms will absorb some of the rubidium light from the lamp, and the light reaching the optical detector will be modulated at the Larmor frequency. The magnitude of the field is computed directly from the frequency measurement. The instrument can be used to measure the direction as well as the magnitude of the field if triaxial biasing coils are placed around the absorption cell. The instrument cannot make absolute vector measurements, since the fields of the biasing coils must be measured or computed.

The rubidium-vapor magnetometer is being used as the basic instrument to survey the geomagnetic field from satellites. It is suitable for field measurements over the entire range of 1 to 20 000 gammas encountered in space applications. Its disadvantages are its temperature sensitivity and its lack of usable output when the ambient field is perpendicular to or parallel to the optical axis.

The helium-vapor magnetometer contains a similar lamp, absorption cell, and optical detector. It operates on the same general principle as the rubidium magnetometer. The variation in light absorption with ambient field is used to servo-control a triaxial set of biasing coils so that the field in the absorption cell remains zero. The vector field is computed from the biasing coil currents, and the instrument does not make absolute measurements.

The helium instrument is designed only for low-field measurements from 0.1 to 150 gammas. Its only use to date has been on the Mariner IV Mars probe. It is quite insensitive to temperature variations, and there are no ambient-field directions for which it has no output.

## REFERENCES

1. CAHILL, L. J., JR.: The Geomagnetic Field. Space Physics, D. P. LeGalley and A. Rosen, eds., John Wiley & Sons, Inc., 1964, pp. 301–349.
2. HOFFMAN, R. A.; AND BRACKEN, P. A.: Magnetic Effects of the Quiet Time Proton Belt. Goddard Space Flight Center Rept. X-611-64-186, 1964.
3. MEAD, G. D.; AND BEARD, D. B.: Shape of the Geomagnetic Field-Solar Wind Boundary. J. Geophys. Res., vol. 69, 1964, p. 1169–1179.
4. MEAD, G. D.: Deformation of the Geomagnetic Field by the Solar Wind. J. Geophys. Res., vol. 69, 1964, p. 1181–1195.

CHAPTER 2

# The Van Allen Radiation Belt

THE VAN ALLEN RADIATION BELT is a doughnut-shaped region surrounding the Earth at the geomagnetic equator, containing energetic protons and electrons trapped in the geomagnetic field. At the geomagnetic equator the region extends from about 1.1 Earth radii from the Earth's center to the magnetopause, where the geomagnetic field is effectively terminated by streams of low-energy particles from the Sun. The position of the magnetopause varies from about 8 to 10 Earth radii. An equatorial section showing the location of the belt with respect to the Earth, the magnetopause, and the Earth-Sun line is shown in figure 2.1.

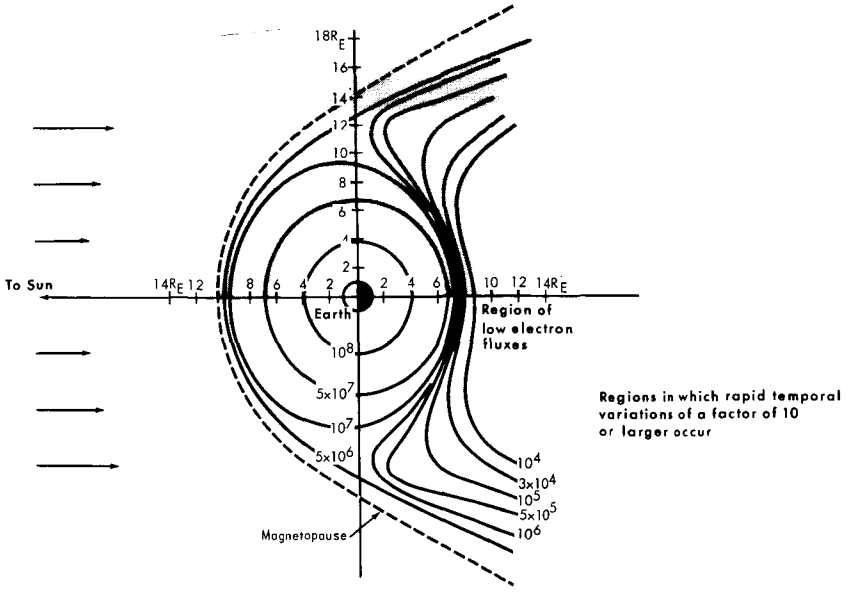


**FIGURE 2.1—The Van Allen radiation belt in the magnetic equatorial plane. Contours show omnidirectional flux of electrons ($E \geq 40$ keV). Outside the magnetosphere, the flux is less than $5 \times 10^2$ electrons/cm²/sec (ref. 1).**

## CHARGED-PARTICLE MOTION IN THE GEOMAGNETIC FIELD

In general, the motion of a charged particle in a magnetic dipole field can be obtained only by numerical integration. For particles whose cyclotron radius is small compared with the scale of the geomagnetic field, the guiding-center approximation may be used to describe the motion. In this approximation the motion is separable into three components.

The first component is a circular motion, perpendicular to the magnetic field lines, with the local cyclotron period $T_1$ and cyclotron radius $R_c$. $T_1$ and $R_c$ are given in Gaussian units by

$$T_1=\frac{2\pi mc}{eB} \qquad R_c=\frac{v_\perp mc}{eB}$$

where $m$, $e$, and $v_\perp$ are, respectively, the particle mass, the particle charge, and the component of the particle velocity perpendicular to the field lines.

The second component is a motion along the field lines in the direction of increasing flux density to a point called the mirror point, at which the particle is reflected, returning to another mirror point, called the conjugate point, in the opposite hemisphere. This oscillatory motion has a period $T_2$ which is substantially longer than $T_1$.

A schematic representation of these two motions is shown in figure 2.2. The pitch angle $\alpha$ of the particle is defined as the instantaneous value of the angle between the particle velocity vector and the direction of the magnetic field; the equatorial pitch angle $\alpha_0$ of a particle is illustrated in figure 2.2.

Since a static magnetic field can do no work on a charged particle, the total energy $E$ of the particle is conserved. In the guiding-center approximation, where the motions are separable, this requires that the total flux through the circular orbit be constant. This is equivalent to the statement, called the first adiabatic invariant of the motion, that

$$\frac{\frac{1}{2}mv_\perp^2}{B}=\frac{\frac{1}{2}mv^2\sin^2\alpha}{B}=\text{Constant} \qquad \text{for nonrelativistic particles}$$

or

$$\frac{p^2\sin^2\alpha}{B}=\text{Constant} \qquad \text{for relativistic particles}$$

where $p$ is the particle momentum. From this invariant it follows that

$$\frac{\sin^2\alpha_1}{B_1}=\frac{\sin^2\alpha_2}{B_2}$$

where the subscripts refer to any pair of points along the particle's

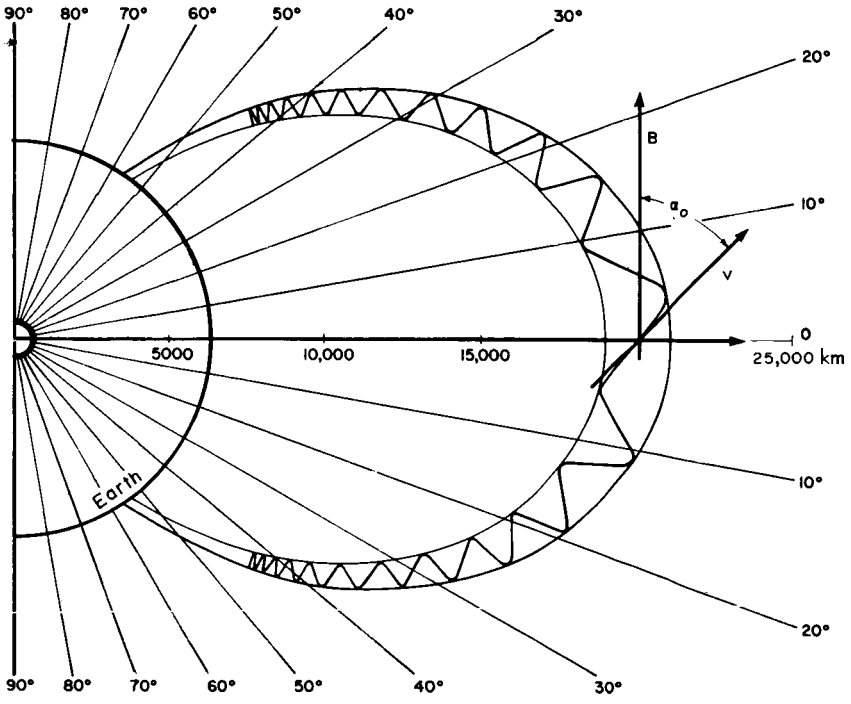


**FIGURE 2.2—Adiabatic motion of charged particles in a magnetic dipole field.**

trajectory. If we choose one of these points at the magnetic equator and the other at the mirror point, it follows that

$$\frac{B_m}{B_0}=\frac{1}{\sin^2 \alpha_0}$$

where $B_m$ is the value of the field at the mirror point and $B_0$ and $\alpha_0$ are equatorial values. Particles which have a value of $\alpha_0$ so small that $B_m$ will be at an altitude of 100 kilometers or less will be rapidly removed by the Earth's atmosphere and such particles must be absent under static conditions. The cone within which such pitch angles are found is called the loss cone.

A particle counter may be used at the geomagnetic equator to measure the unidirectional particle intensity at each pitch angle. The unidirectional intensity as a function of equatorial pitch angle is called the equatorial pitch angle distribution. This distribution, together with the first invariant, may be used to calculate both the unidirectional intensities and the omnidirectional intensity at all points on the same magnetic shell. Alternatively, a particle counter may be used to measure the omnidirectional intensity at every point along a

field line. This description is equivalent to the equatorial pitch angle distribution which may be calculated from it.

A second adiabatic invariant of the motion is associated with the oscillatory motion between the mirror points. It may be stated as

$$J = \oint m v_{\parallel} \mathrm{d}s = \text{Constant}$$

where $v_{\parallel}$ is the component of the particle velocity directed along the field line. The integral is taken along the field line over a complete oscillation of the particle between the mirror points.

The third motion of the particle is a slow drift in longitude with period $T_3$. Electrons drift from west to east and protons from east to west. The particle will slowly transfer itself from one flux tube to another until it finally drifts around the Earth and returns to its original flux tube. In this process it generates what is known as a magnetic shell, surrounding the Earth and open at both ends. A third invariant of the particle motion requires that the total number of lines of flux passing through this shell be constant. This statement is trivial for a static field, and is significant only for slowly varying time-dependent fields.

The guiding-center approximation is thought to describe all the geomagnetically trapped radiation in the absence of strong electric fields or magnetic-field variations which are rapid compared with the characteristic periods $T_1$, $T_2$, and $T_3$. These three periods for typical trapped particles are given in table 2.1.

The particle motion is illustrated in figure 2.2 for a magnetic dipole. Since the geomagnetic field is only approximately a dipole, the particle motion is somewhat irregular even when described in geomagnetic rather than geographic coordinates.

A new coordinate system, defined by using the adiabatic invariants, has been devised to organize particle flux data. The three geographic coordinates $r$, $\lambda$, $\phi$ are transformed into two coordinates $B$ and $L$: $B$ is the scalar value of the field at $r$, $\lambda$, $\phi$; and $L$, given in units of Earth radii, specifies the particular magnetic shell which passes through $r$, $\lambda$, $\phi$. In a dipole field, $L$ would be the geocentric distance to the shell, measured in the geomagnetic equatorial plane. This $L$-shell would be characterized by a certain minimum value of $B$, found on the geomagnetic equator of the shell. In a field which is only approximately a dipole, the same $L$-shell has the same minimum value of $B$, but the trace of this minimum value around the shell is no longer a circle. The value of $B$ at $r$, $\lambda$, $\phi$ is obtained from a spherical harmonic expansion of the geomagnetic field. The value of $L$ at $r$, $\lambda$, $\phi$ is obtained from a relatively lengthy machine computation utilizing the same expansion. A Fortran program for the computation has been widely distributed by McIlwain, who invented the coordinate system.

TABLE 2.1—Gyroradii and periods[a] of the motions of particles in the guiding-center approximation

| | $L=1.5$ | | | |
|---|---|---|---|---|
| | $R_c$, cm | $T_1$, sec | $T_2$, sec | $T_3$, min |
| Electrons: | | | | |
| 50 keV | $4.7\times10^{3}$ | $4.2\times10^{-6}$ | 0.30 | 710 |
| 500 keV | $1.8\times10^{4}$ | $7.7\times10^{-6}$ | .14 | 90 |
| 5 MeV | $1.1\times10^{5}$ | $4.2\times10^{-5}$ | .12 | 12 |
| Protons: | | | | |
| 100 keV | $2.8\times10^{5}$ | $7.1\times10^{-3}$ | 8.4 | 340 |
| 1 MeV | $8.8\times10^{5}$ | $7.1\times10^{-3}$ | 2.7 | 34 |
| 10 MeV | $2.8\times10^{6}$ | $7.2\times10^{-3}$ | .85 | 3.4 |
| 500 MeV | $2.2\times10^{7}$ | $1.1\times10^{-2}$ | .16 | .082 |
| | $L=4.0$ | | | |
| | $R_c$, cm | $T_1$, sec | $T_2$, sec | $T_3$, min |
| Electrons: | | | | |
| 50 keV | $9.0\times10^{4}$ | $8.1\times10^{-5}$ | 0.79 | 270 |
| 500 keV | $3.4\times10^{5}$ | $1.5\times10^{-4}$ | .38 | 34 |
| 5 MeV | $2.1\times10^{6}$ | $7.9\times10^{-4}$ | .33 | 4.6 |
| Protons: | | | | |
| 100 keV | $5.3\times10^{6}$ | $1.3\times10^{-1}$ | 22.0 | 130 |
| 1 MeV | $1.7\times10^{7}$ | $1.3\times10^{-1}$ | 7.1 | 13 |
| 10 MeV | $5.3\times10^{7}$ | $1.4\times10^{-1}$ | 2.3 | 1.3 |
| 500 MeV | ---- | ---- | ---- | ---- |

[a] The gyroradii and periods have been computed according to the formulas of Hamlin, Karplus, Vik, and Watson (ref. 2). A dipole field is assumed. The periods are calculated for particles which mirror at a geomagnetic latitude of 30°. The gyroradius is given for the instant at which the particle crosses the geomagnetic equator.

The value of the coordinate system lies in the fact that the particle intensity (in the absence of time variations and field distortions produced by outside influences) is the same at all points having the same values of $B$ and $L$. For a dipole field, this is simply equivalent to the statement that the particle intensity does not depend on the magnetic longitude. This property of the coordinate system makes possible presentations of particle intensities as a function of only two coordinates $B$ and $L$, rather than the three coordinates which are required to locate a point in space. Since presentations of data in the $B$–$L$ representation do not lend themselves to simple geometric visualiza-

tion, it is sometimes useful to define two dipole coordinates $R$ and $\lambda_M$ according to the relations

$$B = \frac{M}{R^3}\left(4 - \frac{3R}{L}\right)^{1/2}, \qquad R = L\cos^2\lambda_M$$

where $M$ is the magnetic dipole moment of the Earth. This transformation makes possible a dipole-like presentation of the data in $R$–$\lambda_M$ space which permits easy visualization. $R$ is the distance from the dipole source, and $\lambda_M$ is the magnetic latitude. $\lambda_M$ does not differ by more than a few degrees from the usual geomagnetic latitude $\lambda_m$, calculated from an Earth-centered dipole model. A presentation of data in $R$–$\lambda_M$ space is shown in figure 2.3.

### EARLY EXPERIMENTS IN THE RADIATION BELT

The term "Van Allen radiation belt" has historically been used to describe only those particles which have sufficient energy to be detected individually by a radiation counter suitable for use in a space vehicle. This quite arbitrary threshold energy is about 40 keV for electrons, and about 100 keV for protons. The limitation is artificial, and the energy spectra of both types of particles extend downward to thermal energies, where relatively large number densities of protons

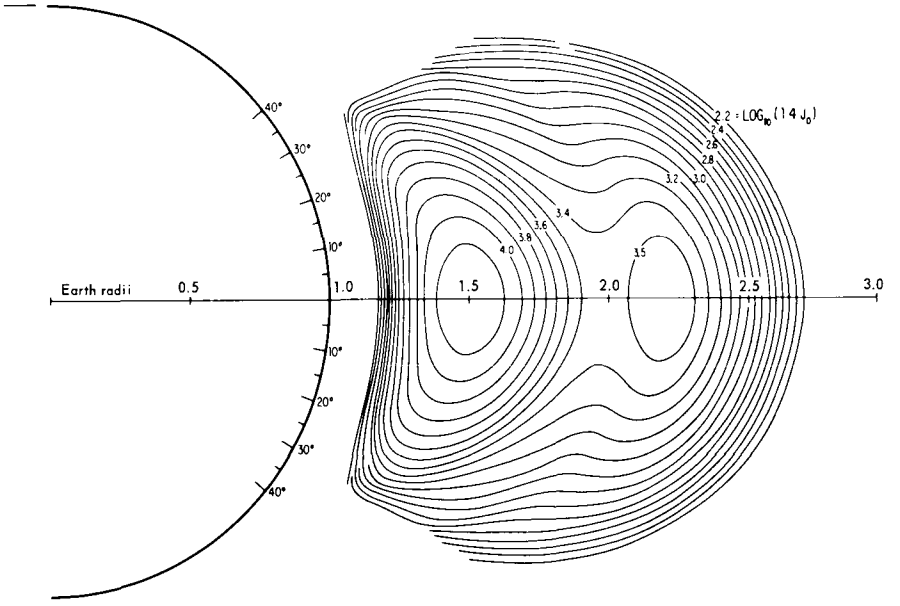


**FIGURE 2.3—Proton flux (40–110 MeV) in idealized dipole coordinates $R$–$\lambda_M$. Contour units are $\log_{10}$ (1.4 $J_0$) (ref. 3).**

and electrons are present everywhere in the exosphere. When thermal particles are included, the number densities of electrons and protons are equal and electrical neutrality is preserved, except perhaps in various transient phenomena.

Although the possibility of trapped radiation in the geomagnetic field has been known for many years, its presence was not established until 1958, when it was first detected by Van Allen and coworkers with instruments on the U.S. satellite Explorer I. Since that time numerous satellite and space-probe measurements have been made by many groups. The interpretation of early experiments was made difficult by the wide range of energies present and by the large time variations which occurred in both the energy spectra and the intensities of the trapped particles. Many early instruments could not distinguish electrons from protons, were often driven beyond their intended ranges, and responded to electron bremsstrahlung, of unknown intensity, produced within the space vehicle.

A number of early experiments indicated the presence of two natural radiation belts, with a region of decreased intensity between them. This apparent structure was to some extent instrumental in nature, caused by a continuous variation of the intensity and energy spectrum of both electrons and protons with distance from the Earth. More discriminating experiments have shown that several particle groups do have two peaks (for example, fig. 2.3). It is possible that other groups may have two (or more) peaks, and that the location of the peaks depends on the particular particle group and may also be time dependent. The division into two belts is most apparent in the measurements of intermediate ($>100$ keV) energy electrons. For these particles, the division appears to be a persistent feature of the radiation belt. The division does not necessarily indicate different origins for the particles in the two zones. In this description the boundary between the zones is taken to be at $L=2$.

### ENERGY SPECTRA AND DISTRIBUTION OF TRAPPED PROTONS

Nuclear-emulsion experiments have indicated that protons make up about 99 percent of the high-energy, positively charged particle flux in the inner radiation zone. Deuterons and tritons make up the remainder. High-energy particles of atomic number 2 or greater have not been detected. While the composition at low energies and in the outer zone has not been determined, most experimenters have assumed that the positively charged particles are protons in these regions as well. A recent experiment indicates that approximately 4 percent of the low-energy, positively charged particles in the outer zone are alpha particles.

Four measurements of the proton energy spectrum at different locations in the radiation belt are shown in figure 2.4. The two curves at $L=1.72$ and $L=1.47$ are representative of the inner zone. These two curves appear to indicate that a relatively strong source of low-energy (5 to 30 MeV) protons contributes to the protons which are trapped on the magnetic shell at 1.72 Earth radii, but not to the one at 1.47 Earth radii. The peak intensity of high-energy protons occurs between $L=1.4$ and $L=1.5$, where the omnidirectional intensity of protons above 40 MeV at the geomagnetic equator is

$$J(>40 \text{ MeV}) = 2\times10^4 \text{ protons cm}^{-2} \text{ sec}^{-1}$$

The two curves at $L=2.8$ and $L=5.0$ are representative of the outer zone. The energy spectrum softens systematically with increasing radial distance in the outer zone, as indicated by the two curves.

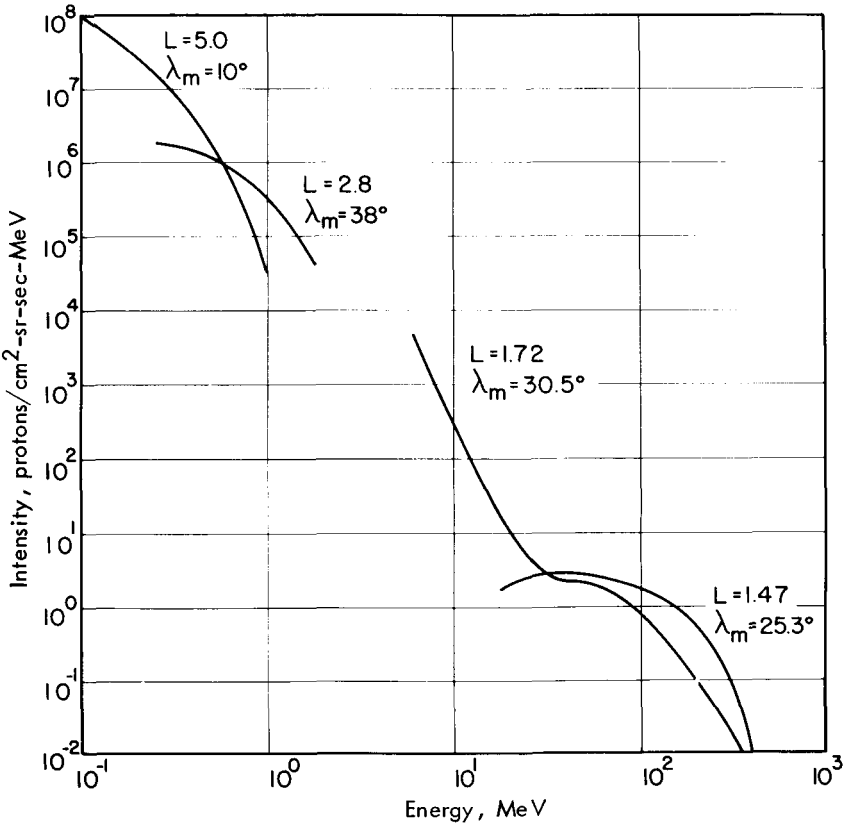


**FIGURE 2.4—Four measured radiation-belt proton spectra. $L$ indicates the magnetic shell and $\lambda_m$ the magnetic latitude. The data at $L = 5.0$ and $L = 2.8$ are from reference 4, at $L = 1.72$ and 1.47 from reference 5.**

The reason for this softening depends on the source and loss mechanisms, which are not well understood. It is believed, however, that protons of tens and hundreds of MeV cannot be trapped in the outer zone because they would violate the adiabatic invariant conditions, and would escape rather quickly from the geomagnetic field even if there were a source to place them there. The peak intensity of low-energy protons in the outer zone occurs at about $L=3.5$, where the unidirectional intensity is

$$j(100 \text{ keV} < E < 4.5 \text{ MeV}) = 6 \times 10^7 \text{ protons cm}^{-2} \text{ sec}^{-1} \text{ sr}^{-1}$$

In addition to these energetic trapped protons, an energy flux of 60 ergs $\text{cm}^{-2}$ $\text{sec}^{-1}$ $\text{sr}^{-1}$ due to protons or positive ions has been detected in the inner zone. This flux is due to protons in the energy range from 400 eV to 500 keV or to positive ions of similar magnetic rigidity.

Figure 2.3 is given as an example of the spatial distribution of the intensities of trapped protons in an energy range in which two peaks appear. Electrons and protons in other energy ranges have intensity distributions which are somewhat similar, but may have greater or lesser extent in both invariant latitude and radial distance, and may have only one peak.

#### ENERGY SPECTRA AND DISTRIBUTION OF TRAPPED ELECTRONS

The omnidirectional intensity of electrons near the geomagnetic equator, having energies greater than 40 keV, is approximately constant within an order of magnitude for $L$ between 2 and 10. The omnidirectional intensity is

$$J(>40 \text{ keV}) \approx 10^7 \text{ electrons cm}^{-2} \text{ sec}^{-1}$$

Electrons having energies from 1 to 5 MeV have a peak intensity in the region near $L=4$, and the electron spectrum becomes progressively softer at greater radial distances. The intensity of the high-energy group can vary by a factor of 1000 or more in connection with disturbances of the geomagnetic field originating in a solar event, but the total intensity of electrons above 40 keV has time variations which are much smaller, perhaps only a factor of 10. An electron spectrum for the outer zone, constructed as a composite of a number of measurements, is shown in figure 2.5.

The natural electrons present in the inner zone were swamped by electrons artificially injected by a nuclear detonation before accurate energy spectra or intensities could be measured. The measurements which were made, however, did indicate that electrons having energies of 1 MeV or more were relatively much less abundant than in the outer zone, and were perhaps entirely absent.

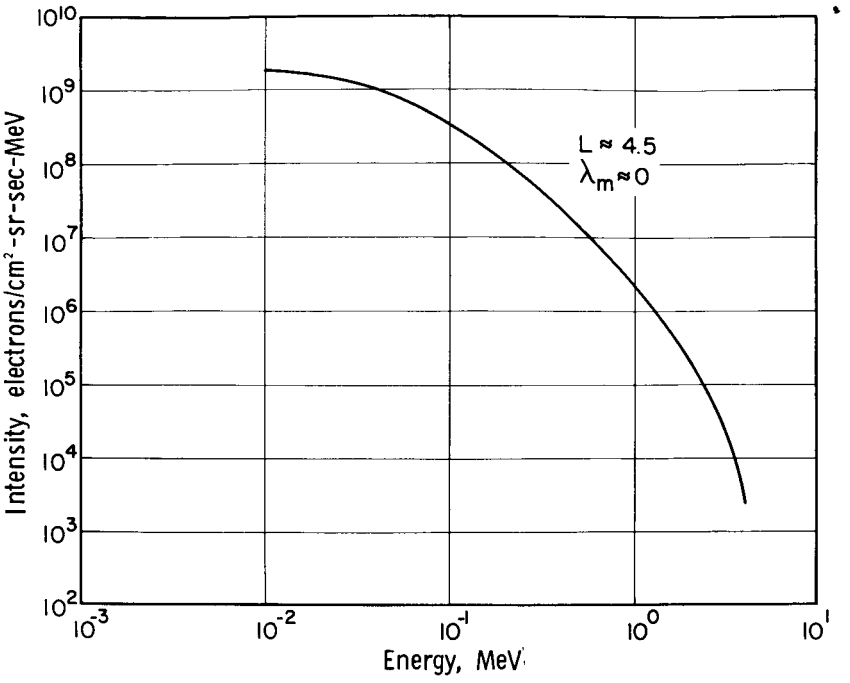


**FIGURE 2.5—Composite electron spectrum near the outer-zone peak-intensity position.**

### SINKS AND SOURCES OF TRAPPED PARTICLES

The intensity of electrons or protons at any given instant at some location in the geomagnetic field represents a balance struck between the mechanisms which are contributing trapped particles and those which are removing them. Evidence indicates that there is more than one significant source and more than one significant sink for each type of particle. If the sources and sinks are approximately constant or slowly varying in time, the intensities will not change rapidly. If either one is impulsive, the intensities will show correspondingly rapid increases or decreases.

The possibility has been considered that the trapped particles may have originated in the Sun, and may have been injected directly into the radiation belt without local acceleration. Such injection is not possible in a static field because particles outside the geomagnetic field cannot enter the trapping region, just as particles inside may not escape. If time-dependent distortions occurred which permitted particles to enter, particles would also escape at the same time. Since deep-space probes have shown that energetic particle intensities in

interplanetary space do not approach those in the trapping regions, even during geomagnetic storms, such a distortion would cause a net loss of particles rather than a gain. The search has therefore turned to more sophisticated and complicated mechanisms.

#### Particle Sinks

While sudden release of trapped particles into interplanetary space due to a gross temporary distortion of the geomagnetic field cannot be ruled out, it is more likely that most trapped particles are lost when their mirror points are lowered to the top of the atmosphere or their energies are lowered below the arbitrarily defined thresholds of the radiation belt. Several sinks which have been considered in some detail are as follows:

##### Collisions with electrons and ions (Coulomb scattering)

This mechanism operates continuously to scatter both electrons and protons of all energies and, in some cases, to cause a significant energy loss of the energetic particle. Electrons are much more likely than protons to have significant angular deflection because of their lower masses. Some of the scattered particles will have lower mirror points than before, and some may therefore be lost in the atmosphere. This is equivalent to the statement that their new pitch angles are within the loss cone. This mechanism acts at all times, but may vary in importance from time to time as the exospheric density changes.

##### Collisions with neutral atoms (ionization-energy loss and charge exchange)

Ionization energy losses are more important than scattering effects for protons. Ionization energy losses of electrons are usually ignored, because they are small when compared with the scattering effects. Charge exchange, a process in which a proton picks up an electron from a thermal atom and becomes a fast neutral atom, is important only for protons below about 200 keV. The frequency of collisions with neutral atoms also depends on the exospheric density.

##### Nuclear collisions

At proton energies above about 80 MeV, nuclear collisions constitute a more important loss mechanism than ionization energy loss, because of the decrease of the latter with increasing proton energy.

#### Scattering by hydromagnetic waves

It has been proposed that hydromagnetic waves propagating inward from the magnetopause scatter high-energy protons and set a maximum value for the proton energy which can be trapped at any $L$-value. The existence of this effect has not yet been verified.

#### Scattering by very-low-frequency electromagnetic radiation (whistlers)

The suggestion has been made that vlf radiation propagating along a line of force may scatter electrons which are trapped along that line, and may even accelerate electrons if synchronism between the electron gyrofrequency and the Doppler-shifted wave frequency can be maintained. It is not known whether a sufficient energy density exists at very low frequencies in the radiation belt to provide either a sink or source of electrons.

#### Acceleration by electric fields

Appropriate electric fields could serve as either a sink or a source, or simultaneously as both. Such electric fields would influence both electrons and protons. The fields might be produced by charge separation or plasma instabilities in the exosphere, either as a local or large-scale phenomenon. The energy for such mechanisms would presumably originate in the particle streams from the Sun (solar wind), or in the rotational energy of the Earth. Since the potential differences across distances the size of the Earth are not likely to be more than $10^5$ volts, such fields are likely to be of importance for low-energy particles only. Production or loss of particles up to 50 to 100 keV of energy might be possible. Specific and detailed mechanisms for producing these electric fields and maintaining them for the required time have not yet been described.

#### Electromagnetic radiation by an accelerated particle (synchrotron radiation)

The maximum energy of a trapped electron is limited by the emission of synchrotron radiation. The limit is probably of the order of tens of MeV in the radiation belt. Synchrotron radiation was observed after the injection of electrons up to about 10 MeV by the nuclear detonation on July 9, 1962. Radio emissions from Jupiter have been tentatively identified as synchrotron emission from electrons trapped in the Jovian magnetic field.

#### Violation of the adiabatic invariants

The treatment of particle motions by the guiding-center approximation requires that the magnetic field have a very small change in a length of 1 gyroradius of any trapped particle. This requirement, instead of hydromagnetic wave scattering, may determine the maximum energy that a proton may have at any given $L$ value. Protons having energies above the maximum would presumably find their way down into the atmosphere or out into interplanetary space within a relatively short time. In addition, the guiding-center approximation requires that any time variations in the field must be slow in comparison to the characteristic periods of the three motions (table 2.1). The third invariant in particular has a period which is long compared with some of the geomagnetic field variations which occur during a geomagnetic storm. There is general agreement that violation of the third invariant will produce a diffusion of particles from a given $L$-shell into adjacent $L$-shells. This diffusion will cause some trapped particles to be lost at the top of the atmosphere and others to be lost to interplanetary space.

It is also possible that violation of the third invariant serves as a source of trapped particles, permitting low-energy solar-wind particles to diffuse into the geomagnetic field from the magnetopause.

### Sources for Trapped Protons

#### Inner zone

Experiments performed since the discovery of the radiation belt have not shown impulsive additions to or losses from the protons above 30 MeV in the inner zone. The variations which have been observed that are not due to experimental differences may have been caused by a redistribution of protons which were already present, or by a slow variation over the solar cycle. The observations are consistent with a weak but approximately constant source at energies above about 30 MeV. These protons may originate in a process, in which very-high-energy (1 BeV or more) galactic cosmic rays strike the Earth's atmosphere and produce neutrons in various nuclear collisions. These neutrons, called albedo neutrons, then diffuse out of the atmosphere and escape from the Earth. A certain fraction of them decay into protons and electrons in the radiation belt. This mechanism is generally thought to contribute at most only a small fraction of the trapped electrons, but it may produce most or all of the high-energy trapped protons in the inner zone. This source may be supplemented at proton energies below about 200 MeV by neutrons emitted by the

Sun and decaying into protons in the inner zone, although solar neutrons have not yet been detected.

The loss mechanisms for these protons are probably ionization energy loss, nuclear collisions, and possibly slow diffusion due to violation of the third adiabatic invariant.

All of these source and loss mechanisms are slowly varying and would produce a trapped proton belt without short-term intensity fluctuations.

At energies below 30 MeV, the proton intensity depends rather strongly on $L$. The energy spectra given in figure 2.4 indicate that there were many more low-energy protons on the shell at $L=1.72$ than there were at $L=1.47$ at the time the measurements were made. Either the source or the sink of these protons must vary strongly with $L$.

It has been suggested that solar cosmic ray neutron albedo would provide a suitable $L$-dependent source. Solar cosmic rays, which are emitted from the Sun during solar flares, typically have energies of several hundred MeV. They are guided into the Earth's polar caps by the Earth's dipole field, and cannot theoretically penetrate into the trapping regions. In the atmosphere above the polar caps they produce neutrons in nuclear collisions in the same way that the higher energy galactic cosmic rays produce them all over the Earth. The protons which are produced by the subsequent neutron decays can be trapped only on $L$-shells for which $L$ exceeds a certain minimum because of the geometrical effect of the source location at the polar caps, and the necessity that the decay proton have a velocity vector which results in a mirror point above the atmosphere. $L$-shells located at low altitudes near the geomagnetic equator cannot be populated by this mechanism.

This source of low-energy protons would be impulsive, since it depends on the irregular occurrence of a solar flare event. Whether this source provides sufficient protons to account for the observations is not known. The loss mechanisms for the low-energy protons are probably the same as those for protons above 30 MeV, and strongly $L$-dependent mechanisms have not been described.

#### Outer zone

It has been proposed that the low-energy protons in the outer zone are supplied by an inward diffusion of solar-wind protons incident upon the magnetosphere at about 10 Earth radii. This diffusion is the result of violation of the third adiabatic invariant by sudden magnetic impulses and disturbances which occur several times daily. Conservation of the first and second adiabatic invariants (which are not vio-

lated because of their much shorter periods) requires that the energies of the protons increase as they diffuse inward. Solar-wind protons having energies of 10 keV or so at the magnetopause would have energies of 10 MeV or more at $L$-values of 3 or 4.

Since the diffusion times increase sharply with decreasing $L$, it is doubtful that this mechanism could supply protons at $L$-values lower than 3 or 4. Loss mechanisms would prevent the very long residence times required to build up an appreciable intensity at lower $L$-values.

Since the intensity of these protons has been observed to increase during a geomagnetic storm, it is tempting to identify them (and possibly lower energy undetected protons) as the source of the "ring current" which causes the main phase depression in the horizontal component of the Earth-surface field. Such a depression typically follows a sudden-commencement geomagnetic storm, and usually lasts for a few days. This may be the time required for the charge-exchange process to remove the excess protons which diffused inward at the start of the storm.

There is not sufficient experimental evidence to verify inward diffusion as the source of these protons, nor to confirm that they are the source of the "ring current."

### Sources for Trapped Electrons

#### Inner zone

The energy spectrum and intensity of electrons in the inner zone was not established unambiguously before the nuclear detonation which took place in the inner zone on July 9, 1962. This detonation injected large numbers of fission-product-decay electrons into trapped orbits and temporarily made study of the natural electrons impossible. Measurements made before the detonation indicated that electrons having energies of 1 MeV or more were few in number, or perhaps entirely absent. The possibility exists that the same neutron decays which produced the energetic protons may have produced the electrons in this region. If they were produced in this way, the energy spectrum should have contained very few electrons above the 780 keV end point of the neutron beta decay spectrum.

The Project Starfish nuclear detonation occurred on July 9, 1962, at an altitude of 400 kilometers above Johnston Island in the Pacific Ocean. Some months later, the measured omnidirectional electron intensities at $L=1.2$ near the geomagnetic equator were

$$J(>500 \text{ keV}) = 3\times10^{9} \text{ electrons cm}^{-2} \text{ sec}^{-1}$$

and

$$J(>5 \text{ MeV}) = 1\times10^{7} \text{ electrons cm}^{-2} \text{ sec}^{-1}$$

The intensity of these electrons is decreasing quite slowly, and some of them will be present for years unless they are lost in some sudden magnetic disturbance. At least six other detonations have taken place at high altitudes at $L$-values of less than 1.2 or more than 1.7. These injections produced observable effects for several weeks at most. Evidently electrons on shells for which $L$ is less than 1.2 are removed rather quickly by atmospheric scattering, while those for which $L$ is greater than 1.7 are removed rather quickly by transient phenomena which are characteristic of the outer zone. The injection of these electrons has tended to obscure the natural processes in the inner zone, but it has certainly established the fact that electron lifetimes in this region are long, and that a weak source would be adequate to populate it. Both the energies and the spatial distribution of these artificial electrons may be substantially modified by natural processes before they are ultimately lost.

#### Outer zone

To understand the source and loss mechanisms for outer-zone electrons, considerable attention has been given to the lifetime of outer-zone electrons. A number of satellite experiments have shown that the intensity of electrons in the heart of the outer zone can remain virtually constant for days at a time. Other measurements, made on high-altitude balloons and low-altitude satellites, have shown large fluxes of electrons pouring downward into the upper atmosphere.

These fluxes have been sufficiently large, particularly at geomagnetically active times, to empty out the portion of the radiation belt which is directly overhead in a time of the order of minutes. This phenomenon, which is called electron precipitation, is almost always present to some extent under lines of force which connect with the outer radiation zone. Since the intensity of trapped electrons is not sufficient to sustain this drain when it is most intense, the precipitated electrons probably are not trapped particles being lost from the outer zone, but are instead fresh particles being accelerated and driven down into the atmosphere by an unknown mechanism. Observations at about 1000-kilometer altitude indicate that when precipitation occurs, the intensity of trapped particles at this altitude increases and becomes approximately equal to the intensity of particles being precipitated. This has been interpreted as evidence that the same mechanism which precipitates electrons also supplies energetic electrons to the radiation belt. Verification of the operation of this mechanism to produce trapped electrons at high altitudes is lacking.

The average rate of energy loss of precipitated electrons in the atmosphere is of the order of $4\times10^{17}$ ergs/sec. This corresponds to

something like 1 percent of the average total kinetic energy which is incident on the magnetosphere in the solar wind. If the solar wind supplies the energy for precipitation, the coupling mechanism must be rather efficient. An alternative source of this energy may be the Earth's axial rotation. Since the plasma trapped in the magnetosphere rotates with the Earth, the diurnal plasma motions caused by the deformation of the magnetosphere by the solar wind may produce electric fields to drive the precipitation. If this is the case, a way must be found for the geomagnetic variations which occur during periods of solar activity to trigger the release of energy from the large reservoir of the Earth's rotational energy, to account for the correlation between geomagnetic activity and electron precipitation. Details of such a mechanism have not been presented.

## INSTRUMENTATION FOR SPACE RADIATION MEASUREMENTS

Many sophisticated techniques for the detection of high-energy charged particles have been developed over the past 40 years. Consequently, a wide variety of instruments were available for use when the Van Allen radiation belt was discovered. Geiger tubes, scintillation counters, and semiconductor-diode counters have all been widely employed. The basic operation of these instruments is not novel and is not discussed here.

Certain special problems have been encountered in radiation belt work, and much effort has gone into instrument designs to solve them.

First, the radiation intensities are very high at the positions of peak intensity, and the radiation comes from all directions. Attempts to shield the detector and allow particles to enter through a small aperture have not been wholly successful because of the rather high intensity of very penetrating particles and the tendency of electrons to produce bremsstrahlung (penetrating X-rays) when stopped in the shield. The problems have been partially solved by instruments with short resolving times to handle the very high rates, with special guard counters to eliminate penetrating particles, and by using counters which are relatively insensitive to X-rays.

Second, there are severe limitations on available power and weight. Semiconductor diode counters have been especially useful because of their small size and weight. A clever scheme has been devised in which two scintillation materials are used with the same photomultiplier tube. It is possible to tell which scintillation material a charged particle traverses by a pulse-shape-discrimination technique employed on the pulses from the photomultiplier tube. This enables one detector to do the work of two or permits a guard counter to be used with one detec-

tor on a single tube. The technique is called phoswich (from phosphor sandwich).

The current need in this field continues to be for instruments whose output can be unambiguously interpreted as the flux of a particular kind of particle in a specific energy range. Such instruments are slowly replacing the simple nonspecific instruments originally employed for these studies. McIlwain has remarked that to determine the electron flux from a bremsstrahlung experiment is about the same as calculating the wind velocity by listening to its roar. Hess has commented that making a quantitative deduction from a phenomenon caused by an unknown number of unidentified particles of uncertain energies is a questionable procedure. The situation is slowly being remedied.

There is also a need for instruments to cover the gap between plasma energies (up to a few keV) and radiation-belt energies (arbitrarily defined here to be those above 40 keV). This energy range is of great importance, but experimental techniques are difficult. This energy range contains particles which are too few in number to be detected by the current which they represent, and too low in energy to be detected individually. New techniques are being developed to close the gap.

## REFERENCES

1. FRANK, L. A.; VAN ALLEN, J. A.; AND MACAGNO, E.: Charged Particle Observations in the Earth's Outer Magnetosphere. J. Geophys. Res., vol. 68, 1963, pp. 3543–3554.
2. HAMLIN, D. A.; KARPLUS, R.; VIK, R. C.; AND WATSON, K. M.: Mirror and Azimuthal Frequencies of Geomagnetically Trapped Particles. J. Geophys. Res., vol. 66, 1961, pp. 1–4.
3. MCILWAIN, C. E.: The Radiation Belts, Natural and Artificial. Science, vol. 142, 1963, pp. 355–361.
4. DAVIS, L. R.; AND WILLIAMSON, J. M.: Low-Energy Trapped Protons. Space Research III, Wolfgang Priester, ed., John Wiley & Sons, Inc., 1963, pp. 365–375.
5. NAUGLE, J. E.; AND KNIFFEN, D. A.: Variations of the Proton Energy Spectrum With Position in the Inner Van Allen Belt. J. Geophys. Res., vol. 68, 1963, pp. 4065–4078.

CHAPTER 3

# The Interplanetary Medium

## COMPOSITION OF THE INTERPLANETARY MEDIUM

THE EASIEST AND SIMPLEST assumption to make about the space in which the planets move in their orbits is that it is empty. Light from the Sun and the stars travels through this space without apparent effect, and planets and comets experience no apparent drag. Certainly the contents of this space, if any, must be of extremely low density and great transparency.

Years before it was possible to probe the interplanetary medium with instrumented spacecraft, a number of phenomena were discovered which were quite sensitive to the composition of the interplanetary medium. It was discovered that the Earth is continually bombarded by high-energy charged particles called cosmic rays. Comets intrude into the interplanetary space, developing tails which exhibit odd behavior. A very small amount of sunlight is scattered to the Earth from directions away from the Sun. The magnetic field of the Earth behaves from time to time as if it is struck by clouds of charged particles. These phenomena served as the first interplanetary probes, and a theory of the interplanetary medium was developed to explain these phenomena.

First, the zodiacal light (see ch. 5) was found to be the result of sunlight scattered from particles of dust. The observation of comet tails provided the solution to the source of the dust: it comes from material ejected from comets as they pass through the inner solar system. The interplanetary medium, therefore, contains dust. The Poynting-Robertson effect (ch. 5) provides a sink for these dust particles, and the present concentration of dust particles represents an equilibrium established between the source and sink mechanisms. The equilibrium concentration is about $10^{-5}$ dust particles per $cm^3$, and this dust is one component of the interplanetary medium.

Most of the other phenomena provided information which suggested that changes were taking place in the interplanetary medium, but gave no information on the steady-state condition of the medium.

The very-high-energy (>1 BeV) cosmic rays of galactic origin which bombard the Earth show a typical lowering of intensity, called a Forbush decrease, whenever a geomagnetic storm occurs. Since the Earth-surface magnetic variations which occur during a storm suggest that charged particles are incident on the magnetosphere, it was supposed that the interplanetary space contained charged-particle clouds at that time and that these clouds were not completely transparent to galactic cosmic rays. To account for this lack of transparency, it was assumed that the charged-particle clouds must contain magnetic fields. It was impossible from these observations to come to any conclusions concerning the scale size of these clouds. At one extreme they might perhaps fill the entire solar system, and at the other extreme be purely local phenomena which the Earth encountered from time to time.

Only one kind of observation permitted the determination of some of the steady-state characteristics of the interplanetary medium. In 1951 Biermann showed that the large accelerations of the Class I comet tails could be accounted for by a rather intense flux of low-energy solar protons blown outward from the Sun. Since such tails are often seen, even in the absence of magnetic storms, this explanation suggested a steady-state ejection of particles from the Sun. Furthermore, cometary orbits are not restricted to the ecliptic plane, and comets sample a very large volume of interplanetary space within a few days or weeks. The persistence of such tails argued for a large-scale ejection of charged particles in all directions from the Sun.

In 1954 Chapman suggested a static model of the Sun's corona in which the charged-particle density was 300 electron-proton pairs per $cm^3$ at the distance of the Earth's orbit. In this model, the Earth is simply inside the coronal atmosphere of the Sun. The theory has certain difficulties in accounting for the observed temperature distribution at the Sun. The observed surface temperature of the Sun is 6000° K, while the lower coronal temperatures are of the order of millions of degrees.

### THE SOLAR WIND

In 1958 Parker suggested that energy could be transferred outward from the coronal base by hydrodynamic streaming of the plasma rather than thermal conduction as in Chapman's model. Parker named the plasma streaming radially outward from the Sun the "solar wind." No serious theoretical objections to this model have been raised, and the experimental observations of the interplanetary medium which have been made on instrumented probes are consistent with it.

The plasma streaming outward from the Sun is continuously accelerated by the pressure gradients within it, and the particles reach the

orbit of the Earth at hypersonic velocities in the range of 300 to 600 km/sec. The object of many experiments has been to determine the characteristics of the steady-state solar wind and the magnetic field which it contains. The characteristics of the wind at the Earth's orbit which have been measured or can be inferred indirectly with considerable assurance are as follows:

| | |
|---|---|
| Particle density, particles/cm³ (of each sign) | 1 to 10 |
| Streaming speed, km/sec | 300 to 600 |
| Temperature, °K | $\approx 10^5$ |
| Particle flux, particles/cm² sec | $\approx 10^8$ |
| Average particle thermal energy, eV | $\approx 10$ |
| Particle mean free path, AU | $\approx 1$ |
| State of ionization, percent | Very nearly 100 |
| Proton total energy, keV | $\approx 1$ |
| Electron total energy, eV | $\approx 10$ |
| Magnetic field, gammas | $\approx 5$ |
| Conductivity, ohm/cm | $\approx 100$ |

The solar wind, with the characteristics listed above, is a highly ionized neutral gas in which most of the ion kinetic energy is associated with the radial streaming and not with thermal (random) motions. The reverse is true for electrons. They have the same streaming speed as the ions, but their kinetic energies due to this motion are much less because of their smaller masses.

The behavior of this gas may be described by the Boltzmann equations which describe the hydrodynamic motion of a fluid. Maxwell's equations must also be satisfied, since the gas particles are charged and are influenced by the electric and magnetic fields which the gas may contain. Such a gas is called a plasma. Plasmas have been studied in the laboratory rather extensively during the past 15 years. Solutions to the equations are not readily obtainable in any but the simplest situation. A considerable amount of information about such systems can be inferred by analogies with the solutions of problems involving ordinary hydrodynamic fluid flow. Conditions corresponding to those in interplanetary space—a hot, streaming, ionized, rarefied gas—are very difficult to reproduce in the laboratory, and only limited insight has been gained from laboratory experiments.

A number of physical arguments may be used, however, to explain some of the main features of the solar wind. A good conductor has the property that it tends to resist any change in the magnetic field within itself. Any small change in the field produces an emf by Faraday's law, and the current driven by this emf opposes the magnetic field change. These currents eventually die out because of the resistance of the medium. The interplanetary medium is such a good conductor, and the scale length is so large, that induced currents do not die out during the time the plasma requires to reach the Earth. The magnetic field

is said to be "frozen" into the medium, and the medium transports the field with its own motion. If the initial field is zero, then the induced currents will maintain zero field.

This physical property of the plasma will have two important consequences. As the plasma streams outward from the corona of the Sun, it will transport with it the magnetic field of that region of the Sun. At large distances from the Sun, the field has its origin in currents within the plasma and not in solar electric currents. But the magnetic flux linking an arbitrary contour which moves with the fluid is the same as it was at the base of the corona.

Furthermore, the outward streaming plasma will sweep any external field ahead of itself in order to prevent any change of field within itself. Physically, this is accomplished by surface currents at the magnetopause which cancel the fields due to external currents at all interior points. It is this plasma property which causes the geomagnetic field to be compressed and confined within a cavity by the solar wind.

### THE INTERPLANETARY MAGNETIC FIELD

According to the solar-wind model of Parker, the solar-wind kinetic energy density is everywhere greater than the magnetic energy density, and the plasma is accelerated radially outward by pressure gradients. The transport by the wind of the solar field (which is approximately a dipole at the solar surface) would result in a radial interplanetary magnetic field were it not for the rotation of the Sun. The rotation of the Sun, to which one end of the field lines is attached, results in a spiral configuration for the interplanetary field. A schematic diagram of this field in the ecliptic plane is shown in figure 3.1. Although the field lines are curved, the plasma velocity is everywhere radial. The configuration is similar to that seen in the pattern of a rotating lawn sprinkler: the water moves radially outward, but the stream of water appears curved.

The stream angle $\psi$, defined as the angle between the field direction and the local radius vector at distance $r$, may be computed from the plasma velocity $v$ and the solar angular velocity $\Omega$. Different portions of a plasma stream leaving the same region of the Sun at different times will be on a spiral. Since the plasma transports the field lines, they must lie along this same spiral if they are still connected to the Sun. Figure 3.2 illustrates the spiral at an instant of time. One portion of plasma emitted at time $t=0$ has reached the point O at distance $r$ from the Sun. Another portion emitted at time $t=(r-\rho)/v$ from the same region of the Sun has reached the distance $\rho$. During

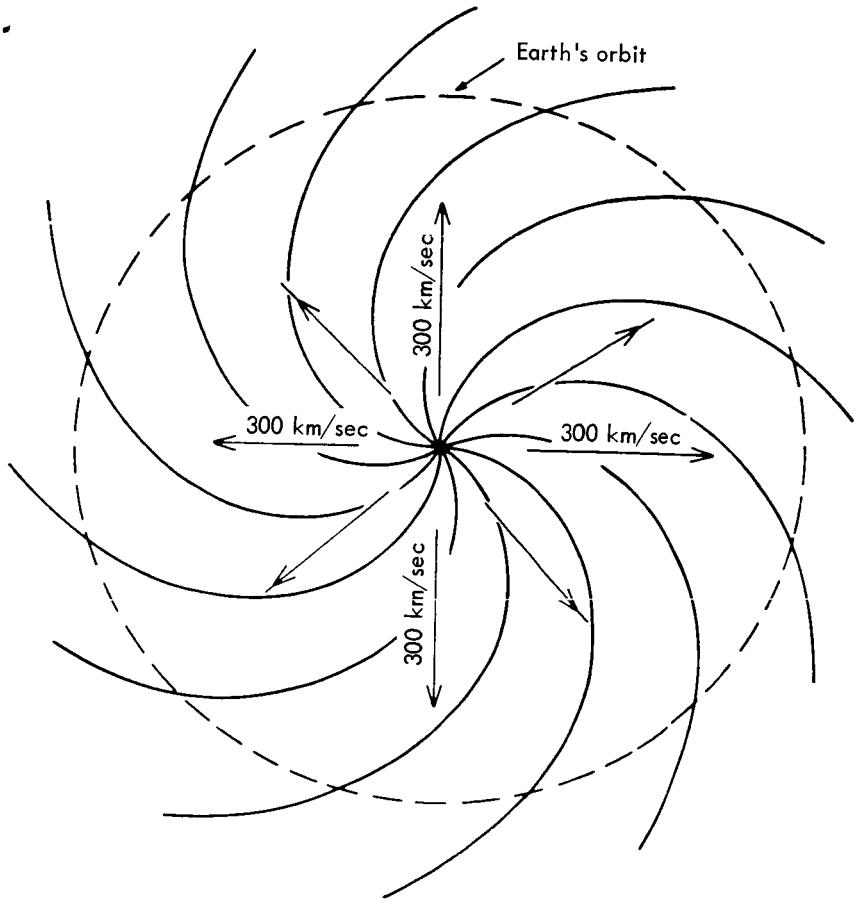


**FIGURE 3.1—Spiral interplanetary magnetic field for a quiet Sun. The plasma velocity is radially directed and is equal to 300 km/sec (ref. 1).**

the time $t$ the Sun rotated through an angle $\phi = \Omega t$. Therefore

$$\phi = \frac{\Omega}{v}(r - \rho)$$

The stream angle $\psi$ at the heliocentric distance $\rho$ will be given by

$$\tan \psi = \rho \frac{d\phi}{d\rho}$$

or

$$\tan \psi = \frac{\Omega \rho}{v}$$

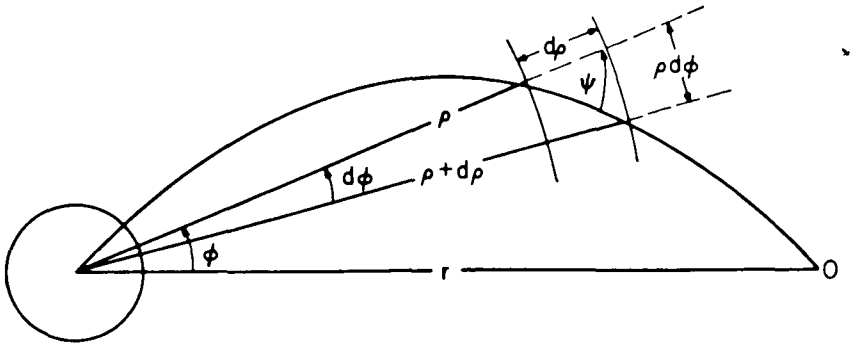


**FIGURE 3.2—Construction for the computation of the stream angle between the radial direction of the plasma and the interplanetary field direction. The plane of the diagram is the solar ecliptic plane (ref. 2).**

Since $\rho$ was chosen arbitrarily, the stream angle at any distance $r$ will be given by

$$\tan \psi = \frac{\Omega r}{v}$$

At a distance $r$ of 1 astronomical unit, corresponding to the Earth's orbit, the stream angle is about 45° for average solar-wind velocities.

This picture of the interplanetary magnetic field is much simplified and does not allow for time variations in solar-wind velocities, departures from radial symmetry of solar-wind emission, and time variations in the solar magnetic field. It may be supposed that figure 3.1 portrays the time-averaged field configuration, while at any given moment much more disorder would exist, as shown, for example, in figure 3.3. Data from Mariner II and Mariner IV, which have observed the field direction over long periods, tend to confirm this more disordered condition.

A second model for the interplanetary magnetic field has been proposed to account for the behavior of solar cosmic rays which bombard the Earth during periods of magnetic disturbance. In this model, proposed by Gold and others, the plasma transports outward a field line bent in a loop with both ends still attached to the Sun. The ends of the field lines may originate in sunspots or in other solar disturbances. The field lines constitute a kind of magnetic "bottle." When this bottle has become large enough to encompass the Earth, the Earth may be bombarded by solar cosmic rays contained within the bottle and may be shielded from galactic cosmic rays which tend to be excluded from the bottle. Both these features of the model are consistent with the observations of cosmic rays during disturbed periods.

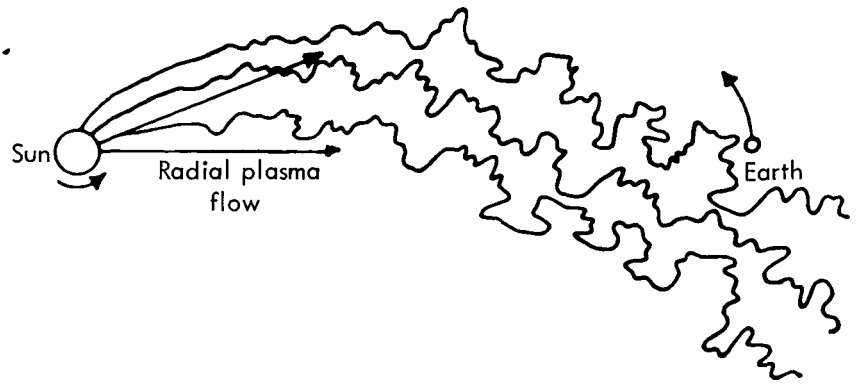


**FIGURE 3.3—Disordered spiral interplanetary magnetic field (ref. 2).**

Parker has suggested the "kink" model for the disturbed period as an alternative to the "bottle" model. In this model the higher velocity plasma associated with the storm condition produces a smaller stream angle of the field as it pushes outward. A sharp kink appears in the interplanetary field lines at the boundary between the fast plasma, and the slower plasma which it is overtaking. The "kink" and "bottle" models are shown in figure 3.4.

It is uncertain which of these models is more nearly correct. It is quite possible that features of both these models may be present during disturbed times. Magnetic "bottles" may also be present during quiet periods superimposed on a generally radial interplanetary field. In all cases the rotation of the Sun produces a spiraling of the field lines at a local stream angle similar to the one obtained in the quiet field model. The models differ chiefly in their large-scale structural features, and it is not easy to distinguish between them with measurements made on a single spacecraft. The small-scale disorder of the field tends to obscure the overall picture. Simultaneous measurements from more than one spacecraft are needed. Cosmic-ray observations are particularly helpful, since they are affected by the large-scale field in a short period as they travel from the Sun to the Earth.

The composition of the ion component of the solar wind is dependent on the mechanism by which it is ejected from the Sun. The approximate composition of the lower solar corona is 10 percent He, 0.6 percent heavy ions, and the remainder protons. If the solar wind were the result of evaporation (thermal expansion) of the corona, severe depletion of the heavy ions would be expected. If it results from hydrodynamic streaming from the corona, the helium may be carried along with the proton stream without significant depletion. Rather uncertain results from Mariner II place the ratio at about 1 percent, indi-

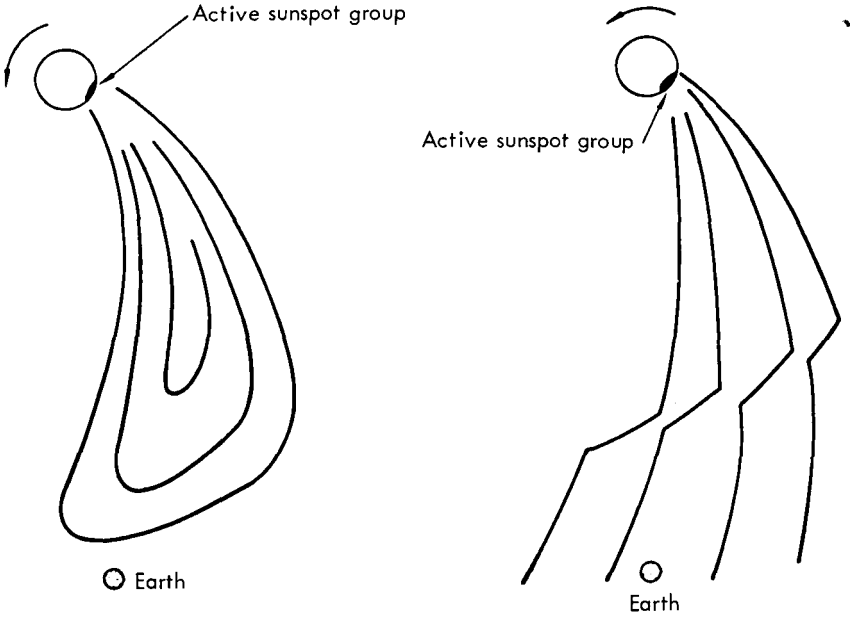


**FIGURE 3.4—The "bottle" and "kink" models of the magnetic field associated with charged particles from solar flares (ref. 3).**

cating some, but not severe, depletion. The effects of this depletion on the theoretical models can be assessed when more accurate measurements are made on Mariner IV and space probes in the interplanetary monitoring platform (IMP) series.

### THE MAGNETOPAUSE AND THE SHOCK STRUCTURE

With this background in the nature of the interplanetary medium, it is possible to understand the rather complex interaction between the solar wind and the Earth's magnetosphere. The solution of this problem presented in chapter 2 assumes that the particles of the solar wind have no transverse velocity component (i.e., a cold plasma) and that there are no interactions between particles (so that a single particle description may be used).

Collisions (Coulomb interactions) between particles are extremely rare, since the mean free path is of the order of the distance from the Sun to the Earth. Neverthless, the particles may interact with each other because they are coupled by the interplanetary magnetic field and by electric fields which may develop. Consider a particle which has undergone a deflection by contact with some obstacle as, for example, the magnetosphere. If its velocity vector after deflection has

a component perpendicular to the interplanetary magnetic field, it will experience a force given by

$$\mathbf{F} = e\mathbf{v} \times \mathbf{B}$$

By Newton's third law the plasma particles in the current which produce the magnetic field **B** must experience the same total force **F**. The plasma particles may then be said to interact with each other because of the presence of the magnetic field. Instabilities which tend to cause charge separation will produce electric fields, and this will also produce group interactions of particles.

It may be supposed that group motions of the particles cannot now be ignored and that solutions which depend on computing individual particle motions are not necessarily valid. The theoretically correct description in the presence of particle interaction is to be obtained from the same hydromagnetic equations required for the solution of the streaming of the solar wind from the corona. The solution of these equations has not been effected in detail, and it is appealing to argue by analogy with ordinary hydrodynamic fluid flow, where particle interactions occur by means of collisions. The resulting description can be at best only qualitatively correct, but it may give considerable insight into the true situation.

In the case of ordinary subsonic fluid flow around an obstacle, wave motion transmits the effect of the obstacle upstream and atoms of the fluid are diverted around the obstacle in some sort of fluid flow pattern. Most of the atoms are never actually in contact with the boundary between the fluid and the obstacle. If the velocity of the fluid with respect to the obstacle is increased, it will eventually reach the phase velocity of waves in the fluid. Above this fluid velocity, waves can no longer propagate upstream in the fluid, and incoming atoms can no longer react to the obstacle at a distance. The solutions of hydrodynamic equations show that a shock front will form as a boundary in front of the obstacle. In front of the boundary, undisturbed supersonic flow exists. Within the shock front a transition to subsonic flow occurs, and the directed particle velocities are converted to random (thermal) velocities. The fluid motion changes from cold supersonic flow to hot subsonic flow. The fluid then moves around the obstacle in the normal subsonic manner.

In constructing an analogy to be used to describe the plasma flow around the magnetosphere, it is necessary to determine whether the plasma is incident at subsonic or supersonic velocities. In general, there are three modes of wave propagation in an ionized gas which contains a magnetic field.

The transverse Alfvén waves propagate along the field direction with a characteristic velocity

$$V_A = (4\pi\rho)^{-1/2}B$$

where $B$ is the unperturbed magnetic induction and $\rho$ is the ionized gas density in gm/cm$^3$. The slow magnetosonic mode propagates in a direction transverse to $B$ with the sound velocity

$$V_s = (\gamma p/\rho)^{1/2}$$

where $\gamma$ is the ratio of the specific heat at constant pressure to the specific heat at constant volume, and $p$ is the gas pressure. The fast magnetosonic mode propagates with a velocity $V_A$ parallel to $B$ and a velocity $(V_A^2+V_s^2)^{1/2}$ perpendicular to $B$. Using the approximate values for the solar wind

$$V_A \approx 100 \text{ km/sec}$$
$$V_s \approx 50 \text{ km/sec}$$

Since the streaming speed of the solar wind is 300–600 km/sec, it is incident on the magnetosphere at supersonic speed with a Mach number of about 5. If the analogy with hydrodynamic flow is valid, a shock wave will be established on the sunward side of the magnetosphere, and thermalization of the plasma (increase in random speed at the expense of streaming speed) will occur there.

Plasma and magnetic field observations in this region tend to confirm this picture in broad outline. A sharp field discontinuity does occur, and the plasma is at least partly thermalized in the region between this discontinuity and the magnetopause. Figure 3.5 shows the magnetic field data of Ness, Scearce, and Seek on a typical crossing of the magnetopause, the shock wave, and a region of interplanetary space. The small spike seen some distance on the sunward side of the boundary, called a precursor, has no hydrodynamic analogy. Its cause is not known. Figure 3.6, from the same authors, is a mapping of many crossings of the shock wave and the magnetopause. The scatter in location of these features from day to day is probably due to variations in the solar-wind pressure. A schematic view of the boundaries in the ecliptic plane is shown in figure 3.7. Note that the solar wind is not incident exactly from the solar direction, but has an aberration of about 5° because of the speed (30 km/sec) of the Earth in its orbit about the Sun.

Since the plasma is at least partly thermalized within the shock front, the shape of the magnetopause will not be the same as it would be if it were determined by a cold streaming plasma. The solution of the Chapman-Ferraro problem given in chapter 1 cannot be a description of the actual boundary. The actual particle pressure at the boundary must be used instead of the pressure calculated from the

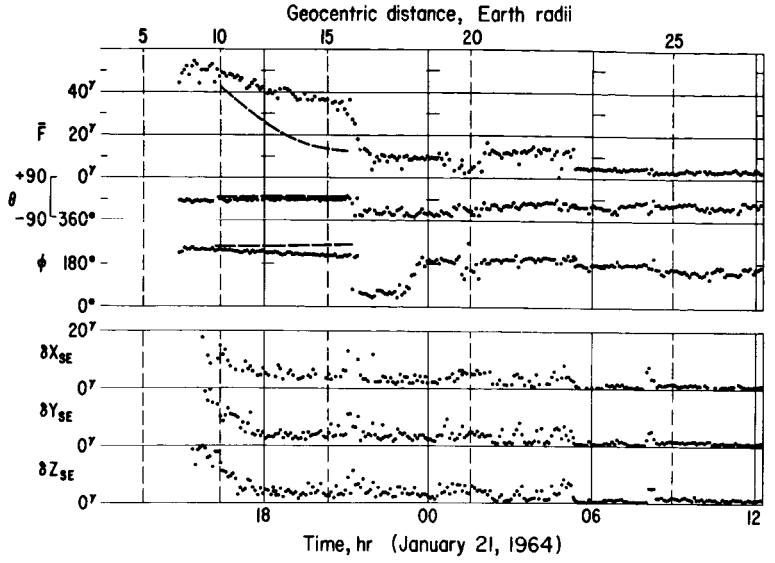


**FIGURE 3.5—Magnetic field measurements from IMP I showing outbound crossing of the magnetopause at 15.7 $R_e$, shock wave at 22.7 $R_e$, and precursor at 24.5 $R_e$. The variances of the X, Y, and Z components of the field in the solar ecliptic plane are indicated by $\delta X_{SE}$, $\delta Y_{SE}$, $\delta Z_{SE}$ (ref. 4).**

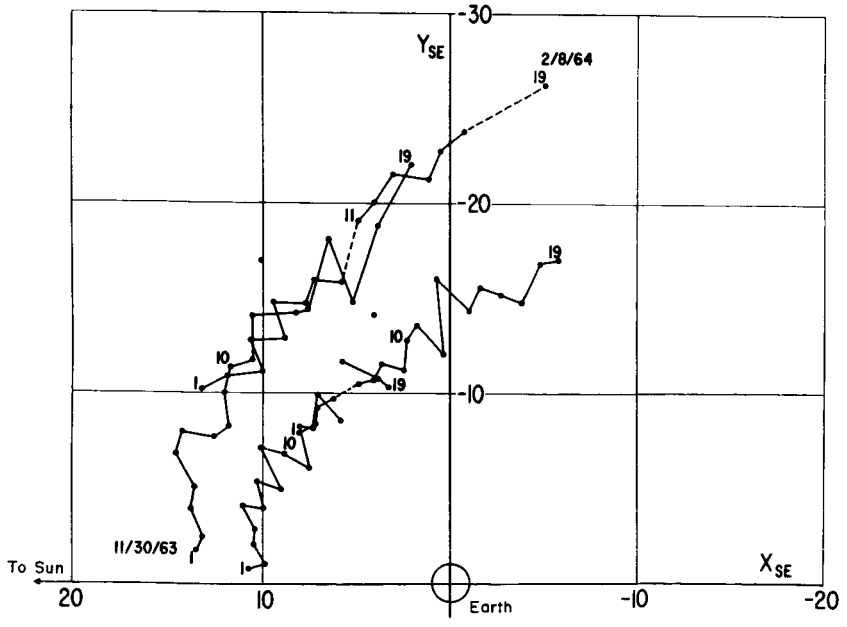


**FIGURE 3.6—Magnetopause and shock-wave crossings rotated into the ecliptic plane (ref. 4).**

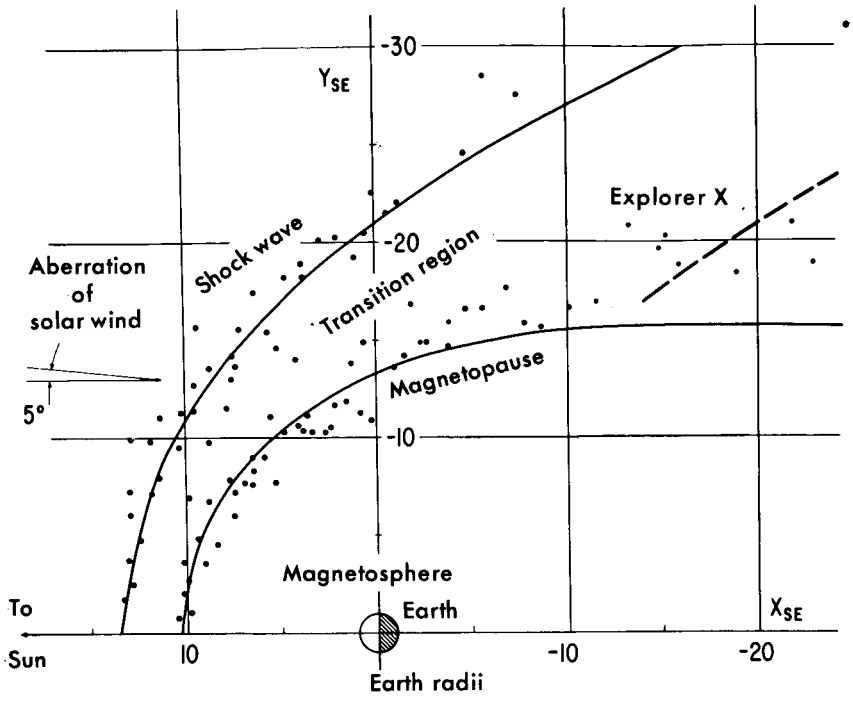


**FIGURE 3.7—Rectified magnetopause and shock-wave crossings by IMP 1, compared with theoretical model from supersonic fluid-flow (ref. 4).**

assumed specular reflection of the incident particles. Nevertheless, the solution of the Chapman-Ferraro problem is at least qualitatively correct, as can be seen by comparing figures 3.7 and 1.7.

### THE TAIL OF THE MAGNETOSPHERE

The tail of the magnetosphere presents a more difficult theoretical problem than the sunward side. A cold streaming plasma will not close the tail at all, because it cannot exert any transverse pressure. In this simple model, the tail is open to infinity. If the plasma is thermalized in the shock front, it can exert a transverse pressure and might be expected to close the magnetosphere at some large distance on the night side of the Earth. The field on the night side would then be confined to a teardrop-shaped cavity.

The actual calculation of the boundary shape must balance all the pressures at the boundary. The external pressure is the sum of the plasma pressure and the interplanetary field pressure. The internal pressure is due to the interior magnetic field, the plasma (if any) con-

tained within the tail, and hydromagnetic waves propagating within the tail. Since several of these pressures are difficult to compute because of a lack of sufficient experimental data, the shape of the magnetospheric tail has not been wholly clarified at the present time.

Dessler has argued that hydromagnetic wave pressure will be sufficient to keep the tail open, even out to distances of many astronomical units, as shown in figure 3.8. Half of the field lines which extend out into the tail come from the Northern Hemisphere, and the lines in this half are directed toward the Earth. The other half come from the Southern Hemisphere and the lines are directed away from the Earth. Between these two portions of the tail is a neutral sheet, or region of zero field, in which the direction of the field reverses. Cross sections of Dessler's model of the tail are shown in figure 3.9. At large distances solar plasma intrudes between the two halves of the tail, and each assumes a circular cross section. The field lines which lie on the surface of these flux tubes are connected to a circle around the Earth at the auroral zone in this model.

Dessler asserts that the daily rotation of the Earth will wind up the

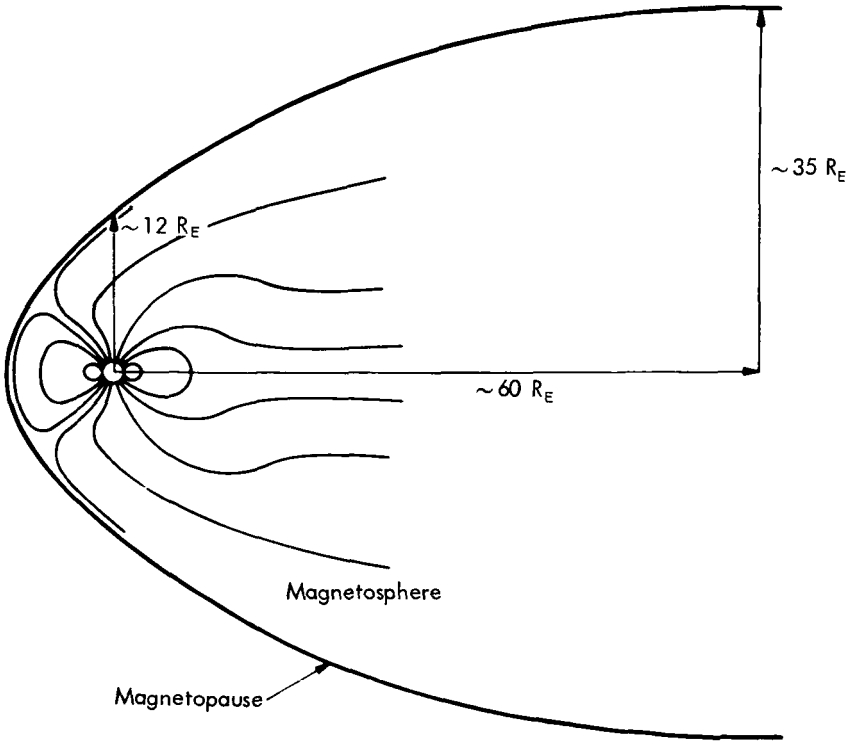


**FIGURE 3.8—Dessler's model of the magnetosphere (ref. 5).**

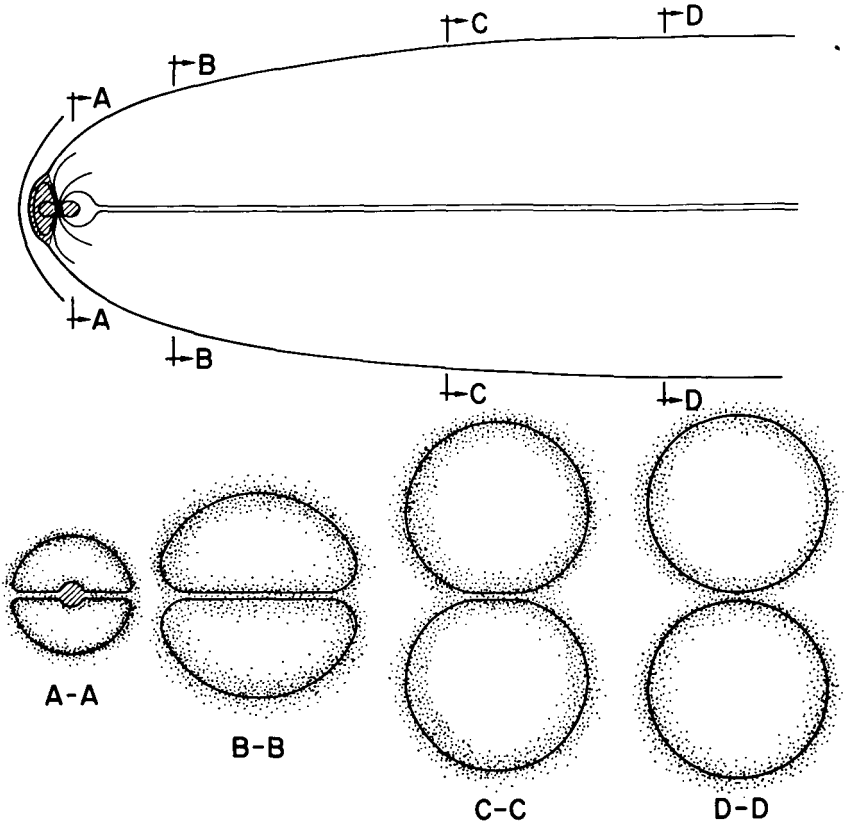


*FIGURE 3.9—Cross sections through the tail of the magnetosphere in Dessler's model (ref. 6).*

field lines in spirals around the flux tubes, just as the rotation of the Sun produces spiral field lines in interplanetary space. This spiraling causes every point on the auroral zones of the Earth to be connected with the magnetopause by a field line which lies along the magnetopause. Viscous interactions between the solar wind and the magnetospheric tail may then, according to Dessler, accelerate particles and drive them down the field lines to produce the aurora.

A somewhat similar configuration of the magnetospheric tail occurs in the model of Axford. Instead of viscous interactions at the boundary, particle acceleration is produced by pressure of the two tail portions on the plasma occupying the neutral sheet between the tail portions, and by shock waves bounding the neutral sheet. This hot, nonthermal plasma is dragged inward by field lines which reconnect across the neutral sheet and move inward toward the Earth. This feature of Axford's model is shown in figure 3.10.

The models of the tail configuration are detailed enough to permit

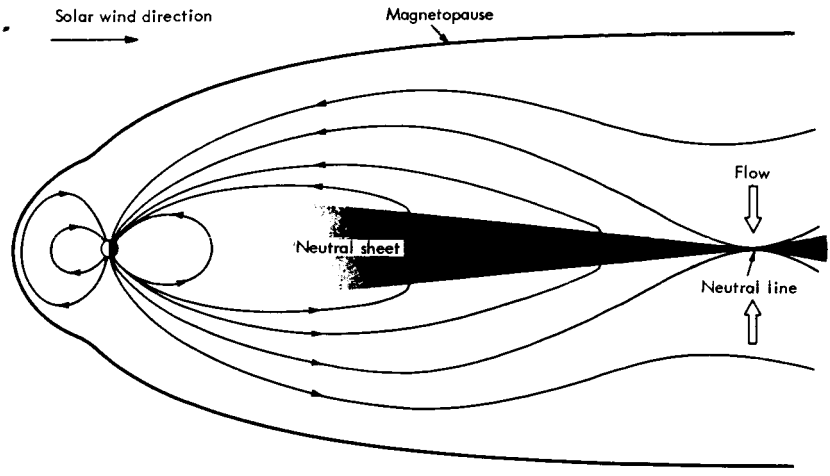


**FIGURE 3.10—Axford's model of the magnetosphere in the noon-midnight meridian. Field lines reconnect across the neutral sheet as the Earth rotates (ref. 7).**

rapid evaluation as soon as adequate measurements are made of the plasma velocities, the plasma density, and the magnetic field within the tail. Such measurements are now being made on IMP, the interplanetary monitoring probe. This Earth satellite has an elliptic orbit of high eccentricity, permitting surveys at all radial distances out to 200 000 kilometers (about 31 Earth radii).

### PLASMA DETECTORS FOR SPACE MEASUREMENTS

Plasma probes are usually devices for collecting charged particles and measuring the current which these particles represent. Certain more sophisticated devices which depend on the transmission characteristics of radiofrequency electromagnetic radiation through a plasma have been designed, but most of the measurements made to date have been with the collection devices. Two simple plasma probes are shown in figure 3.11.

As a result of photoelectric emission from ultraviolet bombardment and excess collection of particles of one sign or the other, a spacecraft may acquire a potential of several volts (positive or negative) with respect to the surrounding plasma. This potential has little effect on the 1-keV ions in the solar wind, but may affect the 10-eV electrons in a drastic way. The spacecraft potential is difficult to measure and even more difficult to control, so that plasma probe devices are customarily used to measure ion densities, velocities, and temperatures.

In order to measure ions, the entrance grid potential is set negative

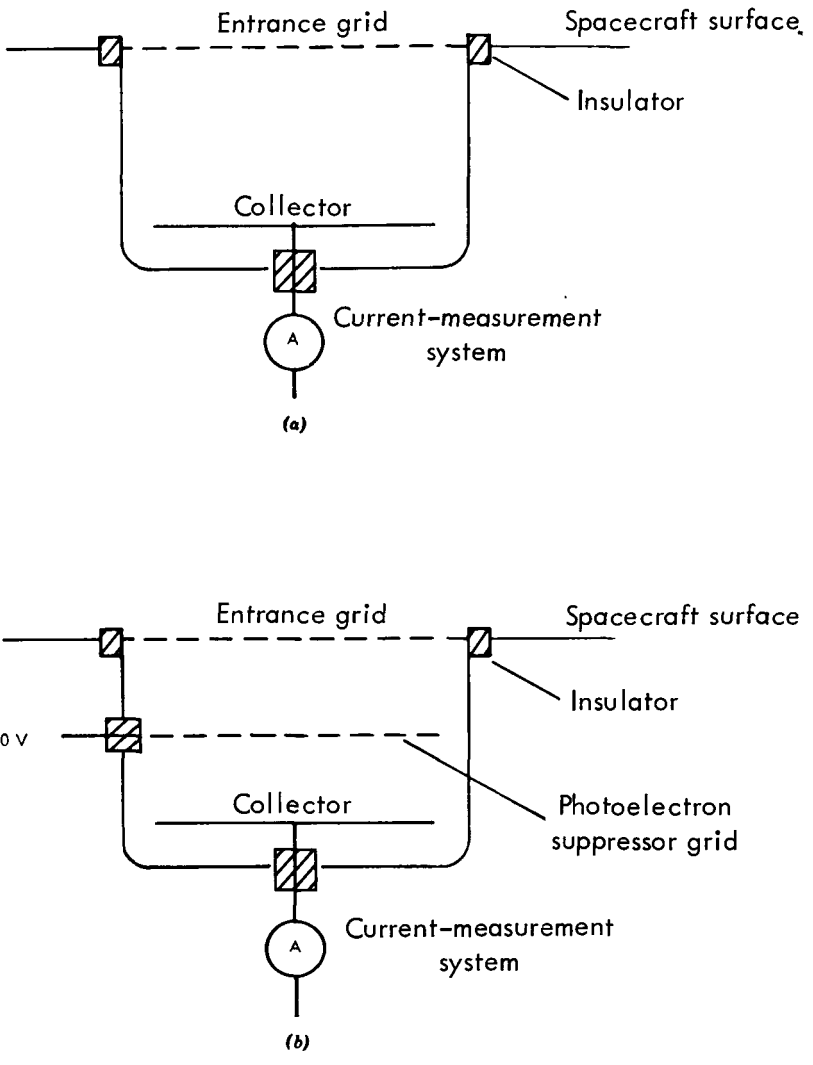


**FIGURE 3.11—Schematic diagrams of two different plasma probes (ref. 8).**

with respect to the spacecraft surface. This prevents the entrance of electrons into the trap. The collector electrode potential is set positive with respect to the entrance grid potential so that the ions which have entered the trap are retarded. Only those ions for which

$$\tfrac{1}{2}mv^2 \cos^2 \theta > ze\ V_{ec}$$

will be collected. The component of ion velocity perpendicular to the spacecraft surface is $v \cos \theta$, the ion charge is $ze$, and the entrance grid-

collector grid potential difference is $V_{ec}$. By varying $V_{ec}$, an integral energy spectrum of the ions may be obtained. The collector current will be

$$I = Nv \cos \theta \, zeA$$

where $N$ is the ion number density and $A$ is the collector area.

The ions in the solar wind are directed radially outward from the Sun, and it is therefore necessary to orient the ion trap directly toward the Sun. Unfortunately, the ultraviolet radiation from the Sun produces photoelectric emission from the collector, and the photoelectric current will dominate the ion current when measurements are made of the solar wind. An electron suppressor grid may be added, as shown in the second trap in figure 3.11, so that the emitted photoelectrons are returned to the collector. This type of probe has been used on several space vehicles. It is limited to fluxes which exceed about $5 \times 10^8$/cm$^2$-sec because of photoelectric emission from the suppressor grid caused by sunlight reflected from the collector. Based on typical solar-wind density and velocity, the solar-wind ion flux is only about $10^8$/cm$^2$-sec, and this design is not suitable for interplanetary measurements.

A more sophisticated ion trap used on Explorer X is shown in figure 3.12. The fourth grid is still used to suppress photoelectrons. The second grid is modulated with a square wave varying between zero and some preset positive voltage $V$. The modulation frequency on Explorer X was 1400 cps. As a consequence of the modulation, singly charged ions of energies up to $V$ electron volts are alternately barred and allowed to pass. The result is an alternating collector signal whose ac component is measured. The photoelectric current is not modulated and has no ac component. It is effectively removed by this technique. The third grid is a shield to prevent capacitive coupling of the modulating voltage to the collector with a consequent modulation of the grid 4 photoelectron current.

The limit of sensitivity of these devices, which is determined by amplifier noise, is about $10^7$/cm$^2$-sec. An integral energy spectrum is obtained by a stepwise variation of the positive modulating voltage. A differential energy spectrum may be obtained if the modulation is varied between two nonzero values.

An entirely different plasma probe is shown in figure 3.13. This device, called an electrostatic analyzer, was used by Snyder and Neugebauer on the Mariner II Venus probe. Only those ions for which

$$\tfrac{1}{2}mv^2 = ze\frac{RV}{d}$$

can traverse a circular path and reach the ion collector. In this equa-

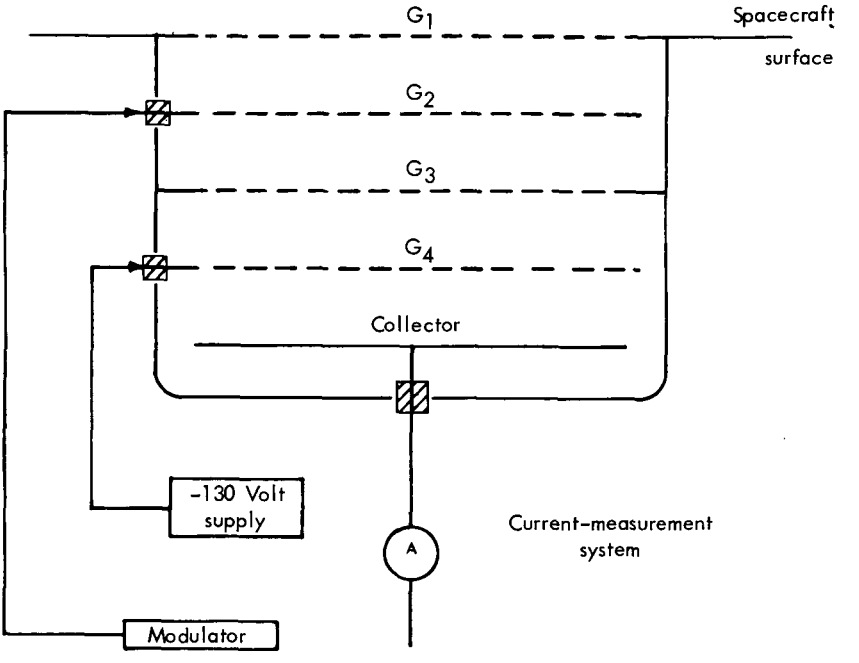


**FIGURE 3.12—Five-element ion trap as used on Explorer X (ref. 9).**

tion, $R$ is the radius of circular path, $V$ is the potential difference between the plates, and $d$ is the distance of separation between plates. The long circular path through an angle of 120° prevents ultraviolet light from reaching the collector except through multiple reflections. A suppressor electrode is used to eliminate the small remaining photoelectric current.

The instrument provides a differential energy spectrum whose resolution at a given energy (full width at half maximum) is about 10 percent. The limit of sensitivity is about $10^6$/cm$^2$-sec, which represents a significant improvement over the ion-trap instruments. A disadvantage of this instrument is its very narrow angle of acceptance; the effective aperture is reduced to about 20 percent of that for normal incidence at an angle of 6°. The motion of the spacecraft transverse to the direction of the Sun introduces an aberration in the plasma velocity, so that it does not arrive at the instrument in the radial direction. This aberration is great enough for low-energy protons that they may fail to be collected at all when the plasma probe is pointed directly at the Sun. A solution is to use more than one analyzer looking in slightly different directions. This not only permits a correction

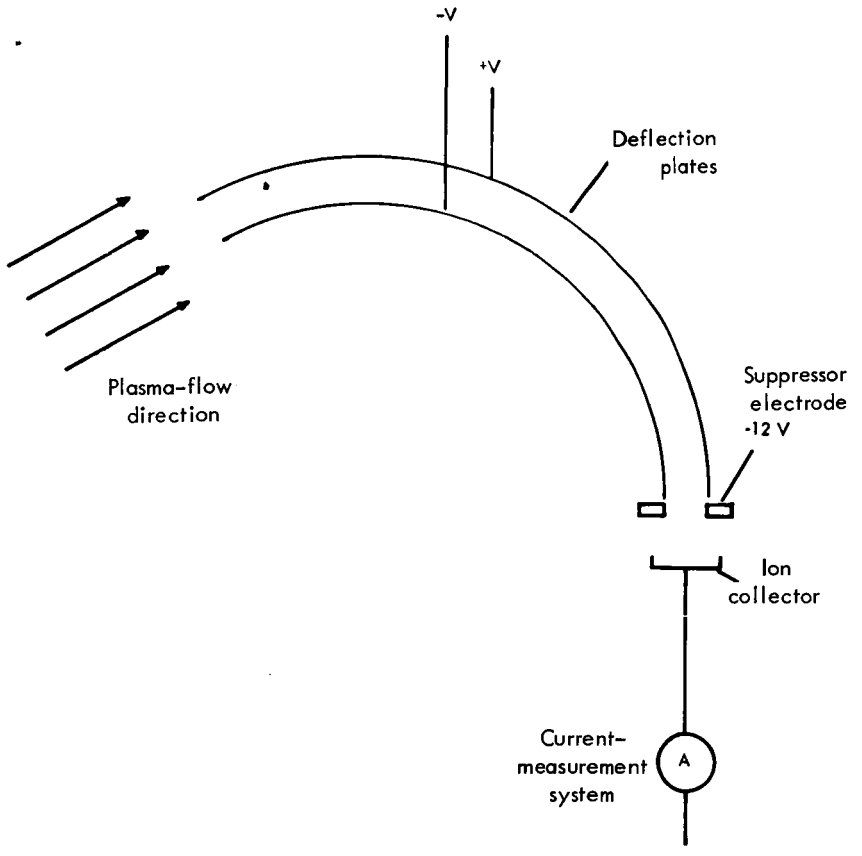


**FIGURE 3.13—Schematic diagram of the electrostatic analyzer plasma probe used in the Mariner II experiment (ref. 8).**

for the aberration to be made, but provides some information about the transverse velocities of the ions, from which their temperature may be computed.

## REFERENCES

1. PARKER, E.: Interplanetary Dynamical Processes. Interscience Publishers, 1963.
2. SMITH, E.: Interplanetary Magnetic Fields. Space Physics. D. P. LeGalley and A. Rosen, eds., John Wiley & Sons, 1964, pp. 350–396.
3. SCARF, F.: The Solar Wind and Its Interaction with Magnetic Fields. Space Physics, D. P. Le Galley and A. Rosen, eds., John Wiley & Sons, Inc., 1964, pp. 437–473.
4. NESS, N. F.; SCEARCE, C. S.; AND SEEK, J. B.: Initial Results of the IMP I Magnetic Field Experiment. J. Geophys. Res., vol. 69, 1964, p. 3531–3569.

5. DESSLER, A. J.: Length of the Magnetospheric Tail. J. Geophys. Res., vol. 69, 1964, p. 3913–3918.
6. DESSLER, A. J.; JUDAY, R. D.: Configuration of Auroral Radiation in Space. Planetary and Space Sci., vol. 13, 1965, pp. 63–72.
7. AXFORD, W. I.; PETSCHEK, H. E.; AND SISCOE, G. L.: Tail of the Magnetosphere. J. Geophys. Res., vol. 70, Letters, 1965, p. 1231–1236.
8. BERNSTEIN, W.: The Solar Plasma—Its Detection, Measurement, and Significance. Space Physics. D. P. LeGalley and A. Rosen, eds., John Wiley & Sons, Inc., 1964, pp. 397–436.
9. BONETTI, A.; BRIDGE, H. S.; ET AL.: Explorer X Plasma Measurements. J. Geophys. Res., vol. 68, 1963, p. 4017–4063.

CHAPTER 4

# Galactic and Solar Cosmic Rays

THE EARTH IS CONTINUOUSLY BOMBARDED by energetic nuclei, electrons, and photons which originate somewhere beyond the magnetosphere. The most energetic of these particles have energies far beyond any produced by any other natural source or by man. They are responsible for sporadic interference with radio communications, for a significant radiation dose to man at sea level, and for the production of $C^{14}$ in the atmosphere. Their origins are not well understood, and their method of production is closely linked with important solar and galactic processes. Until space vehicles became available, these particles had to be studied by indirect means, since they do not penetrate to balloon altitudes without significant interactions with the geomagnetic field and the Earth's atmosphere. They may conveniently be divided into two groups—those which originate in the Sun, and those which do not.

## GALACTIC COSMIC RAYS

Galactic cosmic rays are incident upon the Earth at all times. While the intensity of these particles is modulated by solar activity, it is known that they cannot originate in the Sun. Their energies extend far beyond those which can be produced by solar processes, their directions of arrival indicate that they are not coming from the Sun, and their intensity is greatest during the periods when the Sun is least active. Experiments performed on balloons and on the Earth's surface have determined the intensity, the energy spectrum, the isotopic composition, the directions of arrival, and the time variations of these particles.

### Composition

The galactic cosmic rays are composed of atomic nuclei whose relative abundance roughly parallels the estimated cosmic abundance of these atoms. A measurement made at an energy of 2.4 BeV per nucleon indicates that 94 percent are protons, 5.5 percent are alpha particles, and 0.5 percent are heavier nuclei of atomic number up to 28.

The source of these cosmic rays must accelerate particles with an efficiency that is not strongly mass dependent in order that the relative abundance of the atoms be preserved.

### Energy Spectrum

The energy spectrum of these particles extends upward to at least $10^{19}$ eV, and recent measurements with satellite instruments indicate that there are some galactic cosmic rays with energies as low as $2\times10^{7}$ eV. Except for the very-low-energy end of the spectrum, the kinetic energies of these particles far exceed their rest mass energies, and relativistic dynamics are required to describe their motions. It has been found that the energy spectrum of the protons over a very wide range of energies can be approximately represented as a power law. If $j(\geq T)$ is the flux of protons/m$^2$-sec-sr having total energy greater than $T$, then

$$j(\geq T) = CT^{-\gamma}$$

for an energy range of 1 BeV to $10^{10}$ BeV. The power law fit is not perfect, and the constants $C$ and $\gamma$ must be adjusted for different energy ranges. Figure 4.1 shows a plot of some of the available data. The constant $\gamma$ varies from about 1.4 near 1 BeV to 2.1 near $10^{10}$ BeV. $C$ increases from about $5\times10^{3}$ to $10^{7}$ over this same energy range. The total energy of a relativistic particle is

$$T = Mc^2 = KE + M_0c^2$$

The rest energy $M_0c^2$ of a proton is about 1 BeV. Except for the lowest end of the energy spectrum, this rest energy may be ignored and the total particle energy may be taken as the kinetic energy $KE$.

It has been found that the energy spectra of heavier nuclei also follow a power law, provided that the total energy per nucleon is plotted, rather than the total energy. The nucleon number is the total number of neutrons and protons of which the nucleus is composed. All nuclei which have the same total energy per nucleon have the same velocity, but not the same mass, momentum, total energy, or kinetic energy. Any postulated acceleration mechanism for these particles must be one which will explain this feature of the energy spectra. This feature has not been investigated over a wide energy range because of the difficulty in making identifications of nuclei at very high energies. It may be that more detailed investigation will show deviations from the power law. In any case, it is common practice to compare energy spectra of different nuclei by plotting the total energy per nucleon.

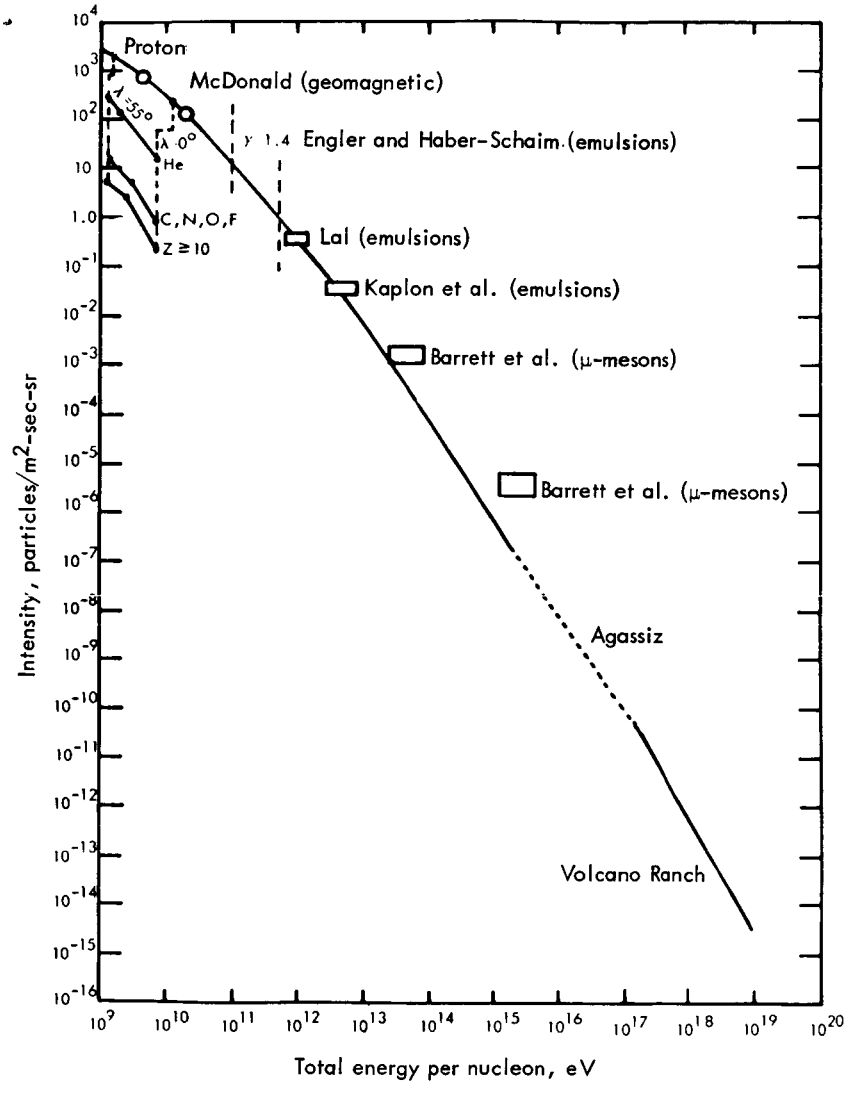


**FIGURE 4.1—Integral energy spectrum of components of the galactic cosmic radiation (ref. 1).**

Another practice with more theoretical justification is the comparison of magnetic rigidity spectra of different nuclei. Most postulated acceleration mechanisms depend upon forces exerted by time-dependent magnetic fields. The magnetic rigidity of a charged particle is the product of the field $B$ and the radius of curvature $\rho$ of the particle in that field.

$$B\rho = \frac{pc}{ze} = \frac{KE}{ze}\left(1+\frac{2M_0c^2}{KE}\right)^{1/2} \qquad \text{(cgs units)}$$

The magnetic rigidity is therefore proportional to the momentum per unit charge. It has the units of gauss-centimeters. As the second expression shows, it also can be expressed in energy units divided by charge units. The magnetic rigidity can therefore be expressed in volts as well as in gauss-centimeters. Conversion between these units may be obtained by dividing volts by 300 to obtain gauss-centimeters. Spectra of galactic cosmic ray particles are often presented as plots of intensity versus rigidity in millions or billions of volts.

Both solar and galactic cosmic rays can reach the top of the Earth's atmosphere only after passing through the geomagnetic field. For each magnetic latitude there exists some minimum energy below which particles cannot arrive at vertical incidence. This energy is called the geomagnetic cutoff. At the geomagnetic equator this minimum energy is about 15 BeV for protons. At the Earth's magnetic poles there is no cutoff, and particles of all energies can arrive, at vertical incidence. The cutoffs may be determined at each latitude by computing the trajectory of a negatively charged particle fired directly upward. If the trajectory intersects the Earth's surface, before the particle escapes from the geomagnetic field, then a positively charged particle of that energy cannot be vertically incident at that latitude.

The computations are materially affected by the field description which is used, and the existence of a ring current or surface currents at the magnetospheric boundary must be properly taken into account. Enhancement of these currents during a geomagnetic storm will substantially reduce the cutoff at a given latitude, permitting lower energy particles to appear at the top of the atmosphere. This effect has been well verified by balloon experiments.

The flux of galactic cosmic rays above 1 BeV is about 0.3 nucleus/cm$^2$-sec-sr. The total energy density of particles above this energy is about $0.4\times10^{-12}$ erg/cm$^3$. This is comparable to the magnetic energy density of the galactic magnetic field, and coincidentally, about equal to the energy density of starlight in our vicinity.

The energy spectrum of galactic cosmic rays below about 1 BeV has been quite difficult to ascertain from balloon measurements, and has been the subject of considerable controversy. Very recent measurements made on the IMP I satellite are shown in figure 4.2. The proton spectrum shows a peak intensity at a rigidity of 1000 MV, corresponding to a kinetic energy of 430 MeV. The last solar cycle minimum occurred during the summer of 1964, and these spectra are therefore characteristic of approaching solar minimum. Some years of further

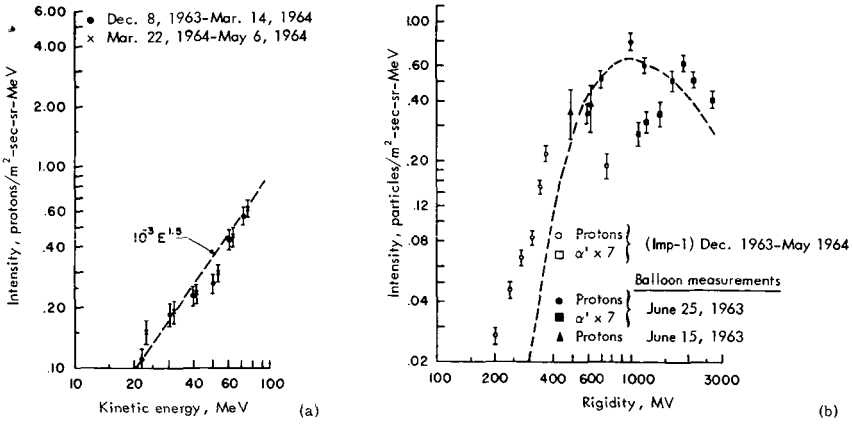


**FIGURE 4.2—(a) Cosmic-ray proton energy spectra at two different times. (b) Rigidity spectra for protons and alpha particles. Balloon measurements at higher energies are included for comparison (ref. 2).**

satellite research will be necessary to define this important low-energy portion of the spectrum over an entire solar cycle.

### Time Variations

The intensity of galactic cosmic rays shows several characteristic time variations, all of which are thought to be local variations in the solar system caused by the activity of the Sun. A pronounced variation is correlated with the 11-year solar cycle, according to balloon and ground station observations. The observations apply mostly to particles having energies greater than 1 BeV. The correlation is rigidity dependent, and the depression in intensity, which is greatest at solar maximum, increases toward lower particle energy at least as fast as the reciprocal of the particle rigidity. The depression at 1 BeV is a factor of about 3 between the period of solar minimum and the period of solar maximum.

This modulation of the intensity by the Sun is the result of the variation in solar corpuscular emission. During periods of maximum solar activity there are many sunspots, frequent solar flares, and copious emission of charged particles. The average solar-wind intensity is high, and the interplanetary magnetic field which it contains is strong. The solar wind expands radially outward, perhaps for hundreds of astronomical units. The interplanetary magnetic field serves as a shield against the penetration of galactic charged particles, and the cosmic-ray intensity decreases. During periods of minimum solar activity, the intensity of the solar wind and the magnitude of the interplanetary

magnetic field are lower, and the cosmic rays can penetrate more readily.

There is a lag of a year or so between the period of minimum solar activity and the occurrence of the galactic-cosmic-ray maximum. This lag is due to the time required for the radially expanding shells of plasma emitted during the last solar maximum to dissipate in the interstellar space. The particle-rigidity dependence of this timelag is useful in the determination of the conditions which exist in the interstellar medium beyond the solar wind. The low-energy particles, which should show the greatest modulation by the solar-activity cycle, have only recently become accessible for study from satellites. It is not known, for example, whether the spectrum shown in figure 4.2 is typical of the interstellar medium, or whether exclusion of these low-energy particles takes place even at solar minimum.

Superimposed upon the 11-year modulation of cosmic-ray intensities by the Sun are short-term variations associated with the enhanced solar corpuscular emission following many (but not all) solar flares. The decrease in intensity which occurs during such a period is called a Forbush decrease after its discoverer. An example of a Forbush decrease as seen by an Earth-surface monitor of cosmic rays is shown in figure 4.3. The onset of a decrease is quite rapid, and the intensity

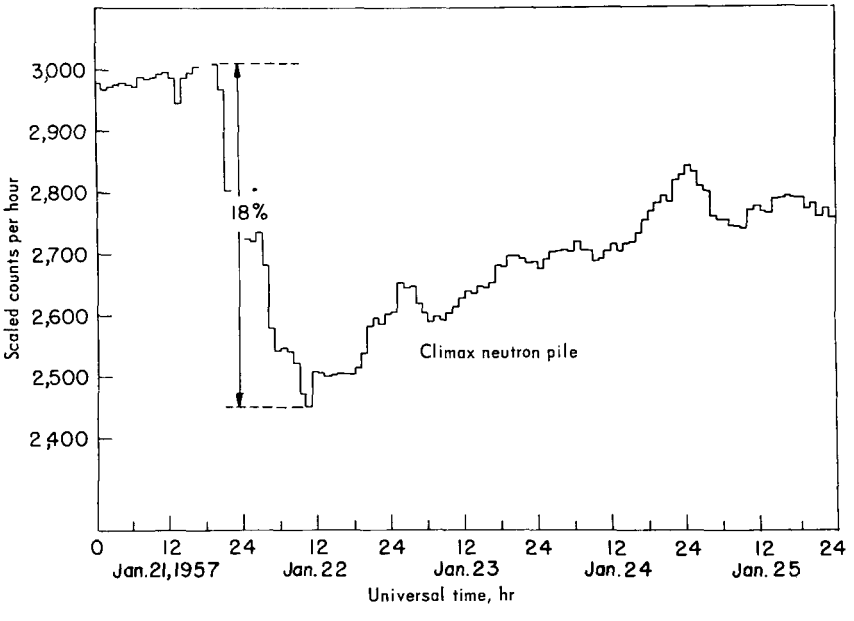


**FIGURE 4.3—The Forbush decrease. A rapid decline in secondary nucleonic component intensity, caused by a change of more than 36 percent in the cosmic-ray flux near the Earth (ref. 3).**

may fall as much as 5 percent per hour. Decreases as great as 40 percent have been observed. The recovery to a normal level is much slower than the decrease and may require many days. The decrease is rigidity dependent for the same reasons that the 11-year modulation is rigidity dependent, although the exact dependence has not yet been determined. It seems likely that the abrupt decrease in intensity is the result of the passage by the Earth of a "kink" in the magnetic field lines at the leading edge of enhanced storm-time plasma overtaking the slower steady-state plasma. The magnetic "kink" is mentioned and illustrated in chapter 3.

A weak flux of high-energy electrons has been discovered whose energies are in the range of several hundred MeV. The intensity is approximately $10^{-2}$/cm$^2$-sec. It is not known whether they are of galactic or solar origin.

#### Origins

The origin of the galactic cosmic rays is highly uncertain. The intensity is very nearly isotropic, and gives no information about the direction of their source. If the energy density of cosmic rays were constant throughout the universe, cosmic rays would be the most abundant form of energy in existence, which appears highly unlikely. It is more reasonable, therefore, to assume that cosmic rays are found only within the galaxies, and not in intergalactic space. A cosmic ray cannot be confined by the galactic magnetic field if its gyroradius exceeds the radius of the galaxy.

For a proton to be stored in the assumed galactic field of $5\times10^{-6}$ gauss, its energy cannot exceed $5\times10^{19}$ eV. Cosmic rays of approximately this energy have been observed. Such events are rare, however. The absence of observations of cosmic rays much above this energy may be due either to their total absence, or simply their very low abundance as predicted by an extrapolation of the energy spectrum observed at lower energies. Long periods of observation will be necessary to resolve this important question.

Cosmic rays cannot be as old as the estimated 8-billion-year age of the galaxy. They must travel very large distances through the tenuous interstellar medium, risking collisions which will fragment the heavy nuclei and slow down the protons. The mean time for a nuclear interaction between a high-energy iron nucleus and a hydrogen atom of the interstellar medium is no more than 20 million years. If cosmic rays were as old as the galaxy, the heavy nuclei would long since have been totally depleted.

The Sun produces cosmic rays from time to time as described below, and it might be supposed that the rest of the stars in the galaxy

produce them at the same average rate. Since solar cosmic rays have never been observed to exceed energies of the order of tens of BeV, it is necessary to have additional acceleration to produce the observed energy spectrum. Such a mechanism has been proposed by Fermi. Even with such a mechanism, production of cosmic rays by all the stars of the galaxy is too low by 6 orders of magnitude to account for the high-energy portion of the observed spectrum.

In the mechanism proposed by Fermi, a charged particle gains energy as a result of a head-on collision with a region of strong magnetic field. Such a process may be thought of simply as the elastic collision of a particle with a massive body moving with respect to the particle. If the body is moving toward the particle, the particle will gain energy. If the body is moving away, the particle will lose energy. The energy gain per collision is small, and the mechanism is very inefficient for nonrelativistic particles. If a proton of energy 1 BeV or more is trapped by a magnetic field between two approaching gas clouds containing strong fields, it can have many collisions as it bounces back and forth, gaining energy in each collision. It is possible that this mechanism could account for the observed intensity and energy spectrum of galactic cosmic rays if there were sufficient low-energy (1 BeV) protons to be accelerated.

Since production by stars like the Sun is inadequate, a search is continuing for objects within the galaxy in which very-high-energy processes are occurring. Such sources are located by detection of electromagnetic radiation, which is unaffected by magnetic fields in the interstellar space. The Crab Nebula, the remains of an old supernova, is an example of such a source. The Crab contains trapped high-energy electrons whose total energy is of the order of $10^{60}$ eV. These electrons emit a great deal of synchrotron radiation, making the Crab Nebula a strong radio source. Supernovae are a possible source of the galactic cosmic rays, although the possibility remains unverified.

Strong radio sources have been detected in other galaxies, and the total energy of the charged particles emitting this radio noise is of the order of $10^{71}$ to $10^{74}$ eV, a truly stupendous figure. Mechanisms for the release of energy in such amounts are highly speculative at the present time.

The opportunity to place instruments outside the Earth's atmosphere makes it possible to extend the observation of the electromagnetic radiation of such sources to X-ray and $\gamma$-ray energies. Early attempts to detect galactic sources of such radiation have not been successful, but more sophisticated and advanced instrumentation is being planned. These experiments can be expected to reveal more of the nature of the very-high-energy processes which are occurring.

## SOLAR COSMIC RAYS

The Sun is a sporadic source of cosmic rays at the lower energy end of the known cosmic-ray spectrum. The production of relativistic (>1 BeV) cosmic rays occurs about once every 2 years, averaged over a complete 11-year solar cycle. About 10 times a year on the average, the Sun emits sufficient nonrelativistic particles to be detected at the Earth's surface by their effects on communications. The particles can reach the top of the atmosphere in the polar regions where the geomagnetic cutoffs are low. The particles enhance the ionization in the D-layer of the polar ionosphere. The enhanced ionization reduces sharply the intensity of galactic radio noise transmitted through the ionosphere. Observation of the transmitted galactic radio noise has proved to be a sensitive method for the detection of solar cosmic rays. The enhanced ionization also absorbs radio signals which are normally reflected from the underside of the ionosphere. This absorption interferes with point-to-point radio communication which depends upon the reception of reflected signals.

The largest solar flare event which has been studied occurred in 1956, when there was a 20-percent increase in cosmic-ray intensity at the geomagnetic equator. The cutoff at the equator at vertical incidence is about 15 BeV. The maximum intensity above an energy of 1 BeV was estimated to be several hundred times the normal flux of galactic cosmic rays.

### Origins

Solar cosmic rays have their origin on the Sun in what is known as a solar flare. A flare is a disturbance which occurs in the solar chromosphere. When it is observed in the light of the hydrogen alpha line, a flare appears as a bright patch on the surface of the Sun, often with bright streamers and loops. The structure grows rapidly and develops with time, rising above the surface of the Sun. A very large flare may have a diameter equal to a fifth of a solar radius or more. A flare may last for several hours, disappearing gradually. Solar flares tend to be associated with active regions on the Sun containing sunspots. Such a region can produce more than one flare during its lifetime.

A solar flare is intimately connected with a strong local solar magnetic field, and observation of the time development of a flare suggests that it is controlled by the field. Time variations in the field heat the solar plasma and accelerate protons and alpha particles to very high energies.

### Geophysical Events Following a Solar Flare

A flare initiates a sequence of geophysical consequences whose time development is illustrated in figure 4.4. The electromagnetic radiations, from radio to X-ray wavelengths, arrive at the Earth simultaneously. The radio emission may persist for days, indicating the persistence of high-energy electrons still trapped in the local solar magnetic field.

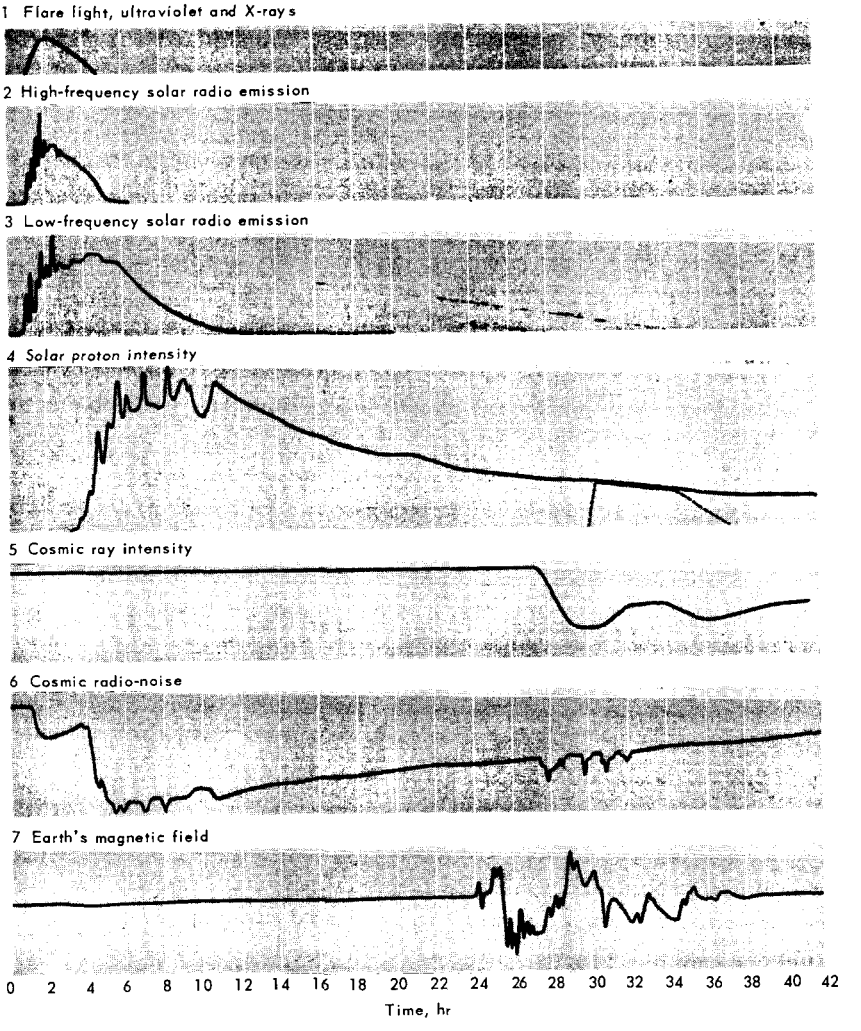


**FIGURE 4.4—Time sequence of geophysical events associated with a solar flare (ref. 4).**

The appearance of highly relativistic solar cosmic rays at the Earth may be almost simultaneous with the optical appearance of the flare. The lower energy protons may be delayed for hours indicating that their paths are much longer than the rectilinear propagation distance from the Sun. This delay may be due in part to the time required for escape from the local solar field, and in part to the diffusion of the particles through the patches of irregular magnetic field between the Sun and the Earth. Figure 4.5 shows the intensity as a function of time after the appearance of X-rays for several proton energy groups. The observations were made from a satellite in nearby interplanetary space. The delayed arrival of the less energetic groups is apparent in the figure.

If the intensity of each group is plotted against the distance traveled before arrival at the Earth, and if the intensity curves are normalized, then the intensity curves overlap, as in figure 4.6. The curves peak at about 10 astronomical units. This indicates that the most probable path length of these particles, over an energy range from 2.2 to 430 MeV, was 10 astronomical units. These long paths must be the result of the diffusion of the particles out of the solar magnetic field, or the diffusion of the particles among the irregular magnetic fields present in interplanetary space.

When plotted in this way, it is evident that the particle energy spectrum is independent of the distance traveled, over a wide range from 2 to more than 100 astronomical units. If this independence may be assumed to hold at zero distance, then the relative intensities of the different energy groups (i.e., the normalizing factors used in fig. 4.6) are a measure of the energy spectrum at the source of the disturbance. The source energy spectrum of this event is fitted very well by the expression

$$\frac{\mathrm{d}J}{\mathrm{d}E} = kE^{-\gamma}$$

where $E$ is the proton kinetic energy, $k$ is a constant, and $\gamma$ is a constant equal to 1.7. Many solar flare events have steeper spectra, with $\gamma$ ranging up to about 4.

The event of September 28, 1961, contained insignificant numbers of relativistic protons, and it is not known whether they will have most probable paths as long as the lower energy particle groups. There is a strong tendency for anisotropy during the early minutes after the arrival of the highest energy proton groups. This appears to be an argument against multiple scatterings in the interplanetary medium for these groups.

Not all solar events produce protons whose arrival times can be so neatly ordered in this way. If a substantial fraction of them can be

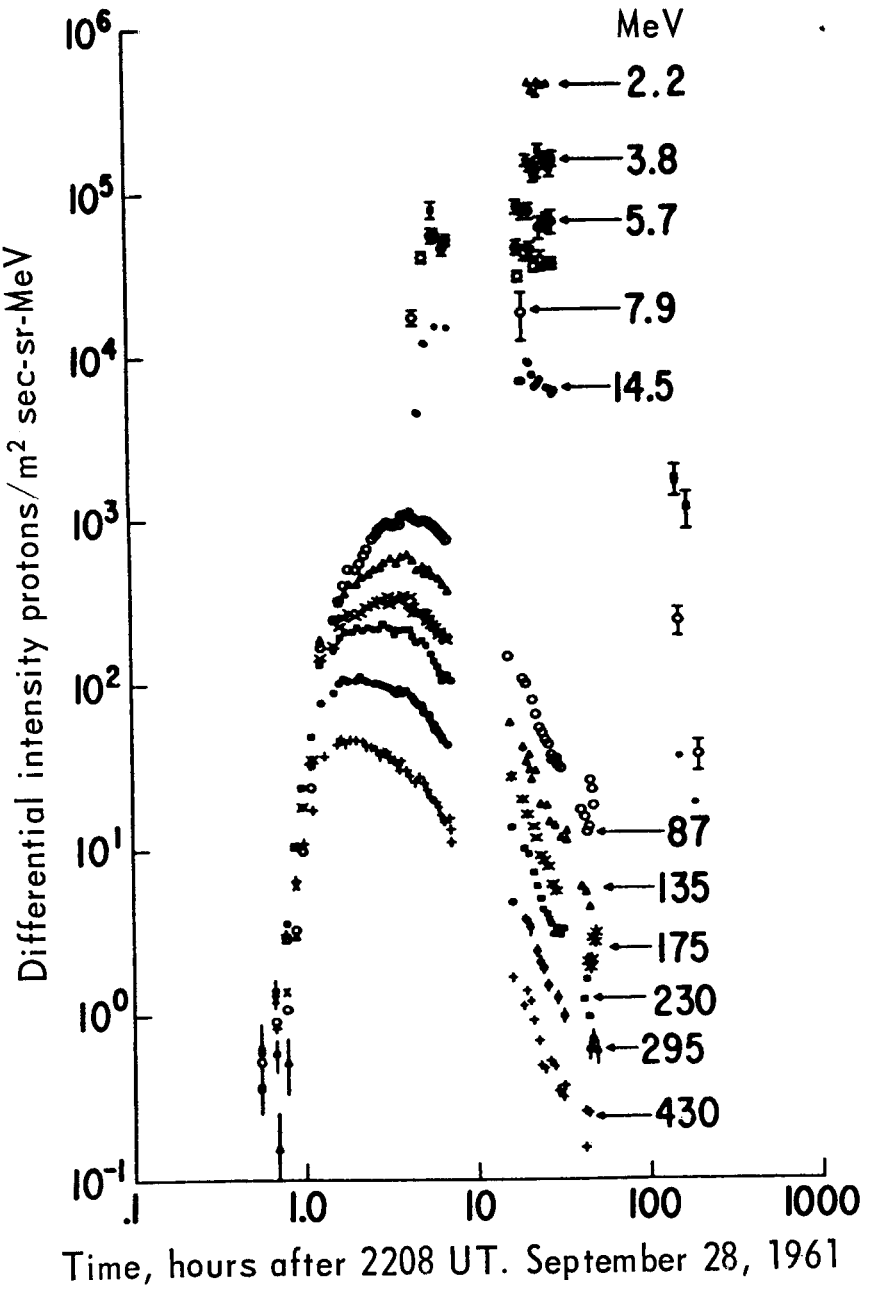


FIGURE 4.5—Differential intensities of solar protons as a function of time after the observance of an X-ray burst associated with a solar flare. Measurements made from a satellite just outside the magnetosphere (ref. 5).

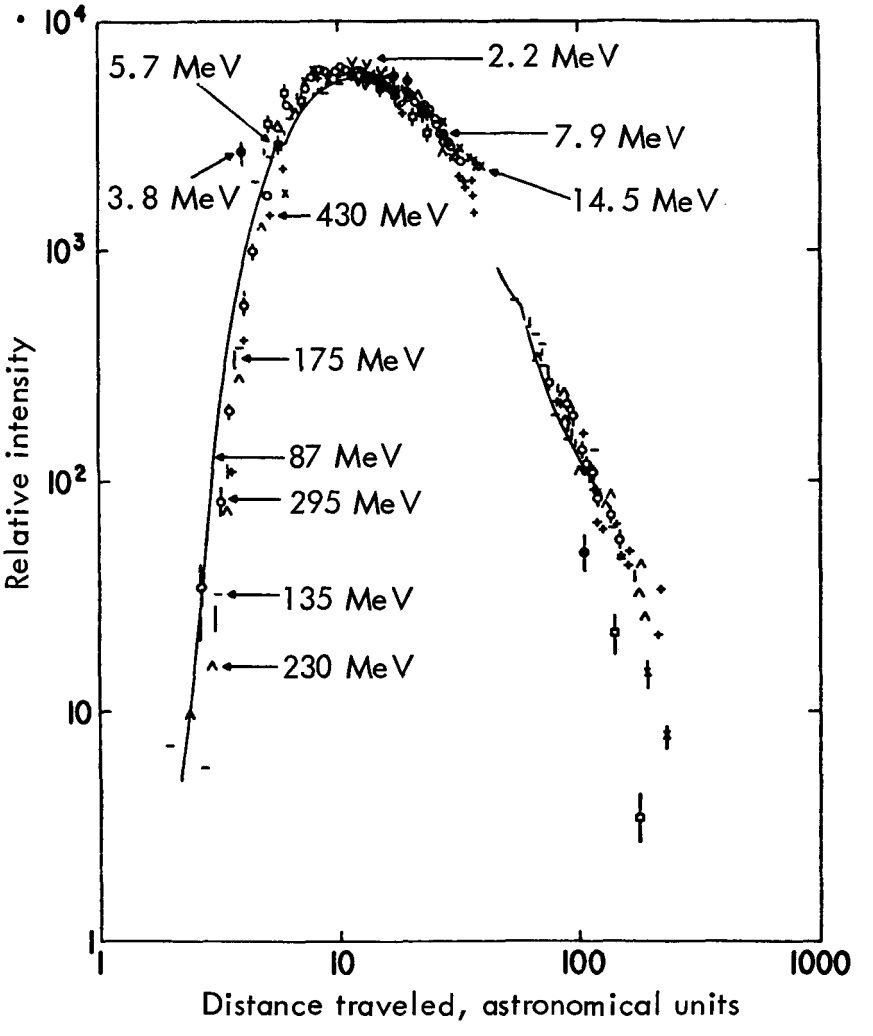


**FIGURE 4.6—Normalized differential intensities of solar protons for the event of September 28, 1961, shown in figure 4.5. The horizontal scale of figure 4.5 is transformed into the horizontal scale of figure 4.6 by multiplying the time of arrival by the velocity of each proton group (ref. 5).**

ordered, however, it will materially reduce the possibilities for the structure of the interplanetary medium.

Some 2 days or so after the occurrence of a flare, an enhanced solar wind reaches the Earth's orbit. Since the enhancement is often restricted to a sector in the ecliptic plane, it is not always observed on the Earth. When this solar wind, enhanced in velocity or density, or both,

does strike the Earth, it produces a geomagnetic storm and a Forbush decrease, both of which are described elsewhere.

The absorption of cosmic radio noise, resulting from ionization by X-rays and ultraviolet radiation, begins at the same time as the optical flare. Further ionization by solar protons increases the absorption. Return to normal follows the decay of the solar proton intensity.

Satellite experiments show that some of the lowest energy solar cosmic rays (1–10 MeV) arrive at the Earth just behind the front of advancing solar wind. They are evidently dammed up by the magnetic field contained in the front, with a diffusion time which is longer than the 2 days or so required for the plasma to reach the Earth. Satellite instrumentation has also discovered the existence of long-lived solar-proton streams which persist for a time greater than the 27-day solar rotation period and reappear after a complete solar rotation. Evidently a storage mechanism exists for long-term storage of such low-energy protons.

### INSTRUMENTATION FOR COSMIC RAY RESEARCH IN SPACE

Well-developed instrumentation for charged-particle research is available for use in studies of cosmic rays as well as of the trapped radiation belt. A number of instruments developed for balloon experiments have proved useful for measurements in space without conceptual modification.

The fundamental problem in cosmic-ray instrumentation is that of measuring the energy and identifying the species of a very low intensity of very penetrating charged particles. The usual technique for such determinations involves the measurement of the rate of energy loss by ionization when such particles pass through matter. More information can be obtained by measuring this loss in two or more layers of matter, often separated by an absorber. The energy loss by ionization depends on the particle charge and particle velocity, and accurate measurements in two or more layers of matter permit both parameters to be determined. Most cosmic-ray experiments represent some compromise between high accuracy and simplicity, and particles are usually sorted into only a few energy and charge groups, depending on the purpose of the experiment.

An arrangement of detectors in layers is called a cosmic-ray telescope, since particles must arrive from a specific solid angle to penetrate all the detectors. Often elaborate coincidence and guard-counter techniques must be employed to prevent interference from particles arriving from other directions, since it is not feasible to shield out such penetrating particles.

The measurement of the low-energy galactic cosmic ray spectrum

has proved especially difficult, since these particles are much less abundant than those of higher energy. Special attention must be paid to production of secondary particles by nuclear collisions of the high-energy particles within the space vehicle and within the instrument itself.

Spacecraft in large-apogee orbits and deep space probes should prove to be ideal monitoring platforms for the observation of solar cosmic rays in a medium where they are undisturbed by the Earth's magnetic field and have suffered no energy loss by passage through the Earth's atmosphere.

## REFERENCES

1. ROSEN, A.; AND VOGL, J. L.: Cosmic Rays in Space. Space Physics, D. P. Le Galley and A. Rosen, eds., John Wiley & Sons, Inc., 1964, pp. 659–704.
2. MCDONALD, F. B.; AND LUDWIG, G. H.: Measurement of Low Energy Primary Cosmic Ray Protons. Goddard Space Flight Center Rept. No. X-611-64-363, 1964.
3. SIMPSON, J. A.: Variations of Solar Origin in the Primary Cosmic Radiation. Astrophys. J. Suppl. Ser. IV, 1960, pp. 378–405.
4. ANDERSON, K. A.: Solar Particles and Cosmic Rays. Sci. Am., vol. 202, no. 6, June 1960, p. 64–71. (Fig. 4.4 p. 66 was reprinted with permission. Copyright (c) 1960 by Scientific American, Inc. All rights reserved.)
5. BRYANT, D. A.; CLINE, T. L.; DESAI, U. D.; AND MCDONALD, F. B.: Studies of Solar Protons With Explorers XII and XIV. Astrophys. J., vol. 141, 1965, pp. 478–499.

CHAPTER 5

# Comets and Dust

## THE ORBITS OF COMETS

THE APPEARANCE OF A COMET bright enough to produce a spectacular sight in the night sky is a relatively rare event. Since this phenomenon can be observed by everyone, its occurrence has usually become a part of the recorded history of its time. Records indicate that Halley's comet, whose period is 76 years, has been observed to return to perihelion no less than 29 times.

In this respect Halley's comet is something of an exception. The *Catalogue of Cometary Orbits,* published by the British Astonomical Association (1961), lists the elements of 829 orbits, determined on 566 individual comets. The list includes 54 individual short-period comets (periods of less than 200 years), of which there have been 317 apparitions, 40 short-period comets of a single apparition, 117 long-period comets, 290 comets with apparently parabolic orbits, and 65 with apparently hyperbolic orbits. The majority of comets, then, are seen only once.

To determine what the orbits of the comets were like before they had been perturbed by the planets, the orbit may be integrated backward through time, including all the perturbations. These computations, with few exceptions, indicate that all of the comets with hyperbolic, parabolic, or long-period elliptical orbits approached the solar system in elliptic orbits with aphelia in the range of 30 000 to 100 000 astronomical units. Consequently, it is believed that comets are permanent members of the solar system whose orbits extend a significant fraction of the distance to the nearby stars.

In this very large volume of space so far from the Sun, stellar perturbations will have a significant effect on the cometary orbits. From time to time the effect will be to alter the perihelion of the orbit to a few astronomical units and the comet will appear in the inner solar system. A passage so close to the Sun is often disastrous, to judge by the disappearance of many short-period comets after one or a few passages through perihelion in the inner solar system.

It appears likely that the short-period comets originate in the same reservoir, between 30 000 and 100 000 astronomical units, but have suffered fairly large perturbations by the planets, drastically reducing their aphelia. Since Jupiter contains most of the mass of the solar system which is not in the Sun, it is chiefly responsible for these perturbations. The perturbations have a random effect, and about half the comets leave the solar system in hyperbolic orbits, while the other half are shifted into shorter period elliptical orbits.

This general picture of cometary orbits depends upon the observed orbits and the computed perturbations. It has been suggested by Beard that the orbit determinations are unsatisfactory because they do not take into account the loss of mass by evaporation as the comet nears the Sun. Because of the large uncertainty in rate of loss of mass, it is difficult, if not impossible, to correct for this effect.

### THE STRUCTURE AND COMPOSITION OF COMETS

At large distances from the Sun, a comet, if it can be seen at all, appears as a dim object without the structure which develops as it moves closer to the Sun. When it approaches to the order of 10 astronomical units, a comet gradually brightens, takes on a diffuse appearance, and sometimes, at a distance of about 2 astronomical units, develops one or more tails. The change is believed to be due to evaporation of material from the comet as it is heated by solar radiation. Comets which have been discovered in recent years are often faint telescopic objects which are too remote from the Sun or too poor in volatile materials to develop these basic cometary characteristics.

The coma, or diffuse area around the cometary nucleus, shows spectroscopic evidence of the neutral molecules CN, $C_2$, $C_3$, OH, NH, $NH_2$, CH, and atomic oxygen. At small heliocentric distances (less than 0.7 astronomical unit) the atomic lines of Na, Fe, and Ni have been identified. It is likely that the molecular lines are the result of the evaporation and photodissociation of $H_2O$, $NH_3$, $CH_4$, and $CO_2$. The atomic lines of Na, Fe, and Ni appear when the comet approaches the Sun sufficiently close to cause appreciable evaporation of these substances.

Study of the tails developed by comets, which in exceptional instances may be more than 150 000 000 kilometers in length, show them to be of two types—dust tails and ionized-gas tails. Since the forces acting on the dust and on the ionized gases are substantially different, these materials are quickly separated as they leave the comet coma, and trail outward in different directions. Many comets do not have both types of tails.

Dust tails are often strongly curved. The orbits of the particles of

which they are composed can be adequately accounted for by the assumption that they are solid particles attracted toward the Sun by gravitational forces, while being simultaneously repelled from the Sun by the pressure of solar radiation. The light from the dust tails consists of scattered sunlight. The variation in scattering efficiency with wavelength has indicated, for two typical comet dust tails, that the diameters of the individual dust particles are of the order of 0.25 to 5 microns. If the particles are assumed to be iron spheres of diameter near 0.6 micron, the brightness measurements indicate an average separation of 4.2 meters for the particles which made up the tail of these comets. The dust tails typically show little structure or rapid time development. Their direction is generally outward from the Sun.

In contrast to the dust tails, the ionized-gas tails are very nearly straight. Observations of the motion of the structures which they often contain indicate very high accelerations which must be caused by forces which exceed the Sun's gravitational force by several orders of magnitude. Spectroscopic observation of the light from these tails shows the band spectra of the ionized gases $CO^+$, $N_2^+$, $CO_2^+$, $CH^+$, and perhaps $OH^+$.

The forces which are responsible for these large accelerations are believed to be the pressure from the ionized solar plasma stream and the solar magnetic field which it contains. This plasma stream, or solar wind, is emitted continuously by the Sun. It has been suggested that the plasma stream may account both for the ionization of the gases and the forces which act upon the ions in the tail. Gas tails often extend radially for millions of kilometers and, on rare occasions, hundreds of millions of kilometers. In spite of this very large extent, their transverse dimensions are often small and well maintained even during rapid motion of the tail. The directions of the ionized-gas tails are thought to be determined by the direction of the solar plasma stream (solar wind) and the magnetic field which it contains. This direction is usually not more than a few degrees away from the Sun direction. The magnetic field is thought to be responsible for the confinement of the gases to a narrow tail, since the ions can drift only very slowly in a direction transverse to a magnetic field.

The mass of a cometary nucleus must be estimated from indirect measurements. The solid nucleus of Halley's comet has been estimated to have a radius between 1.5 and 20 kilometers. The estimates have been made from its brightness at large solar distances where ejected material does not contribute to the reflected light, and from estimates of the rate at which it loses material during each pass through perihelion. Since Halley's comet is much brighter than the average comet, it is reasonable to suppose that the average comet on its first apparition has a radius of about 300 meters.

Whipple has proposed that the solid comet nucleus is made up largely of icy solids in which are embedded solid dust particles of higher density. In this model the vaporization of the icy matrix of frozen water, methane, ammonia, and other substances takes place when the nucleus is heated by solar radiation, releasing the embedded dust particles. This model is reasonably successful in accounting for the appearance of the large quantities of dust and gas as the comet nears the Sun. The model predicts a density of the order of 1.3 gm/cm$^3$ for the entire solid body.

### THE ORIGIN OF COMETS

Theories of the origin of comets are unsatisfactory at present. It is possible that comets are as old as the solar system, and were formed at the same time as the planets. It is also possible that they represent accretions of solid matter which continue to grow in size during the long years they spend in the dark regions of the solar system. Such accretion does not seem likely to occur by gravitational forces alone, but it is possible that bombardment by particles in the solar wind may cause the comet to acquire an electric charge which attracts dust particles to the comet nucleus.

A valuable scientific experiment could be performed by a space probe designed to pass through or land on a comet. The problems are formidable because of the short time in which the cometary orbit must be determined with high accuracy, and the high energy necessary to match an orbit far different from that of the Earth.

### THE CONCENTRATION OF DUST IN THE INNER SOLAR SYSTEM

There is observational evidence which permits an estimate to be made of the density of interplanetary dust. First, the solar corona, which can be seen as a bright halo around the Sun during a solar eclipse, is asymmetric. It extends farther from the Sun in the plane of motion of the planets. This asymmetry is due to the diffraction of sunlight by dust particles larger than a few microns. From the measured intensity of this scattered sunlight, it is possible to estimate the density of dust in the inner solar system. At the position of the Earth's orbit, this estimate is of the order of $10^{-5}$ particles/cm$^3$. The exact concentration depends on the presently unknown minimum particle size.

Observation of a second optical phenomenon, the zodiacal light, permits an independent estimate to be made. The zodiacal light is a faint sky light noticeable in the post-twilight period, concentrated in the plane of motion of the planets. This light is produced by sunlight reflected from dust particles. Numerical estimates of the dust con-

centration from this phenomenon are in agreement with those made from coronal observations, provided that the minimum particle size is of the order of a few microns.

These dust particles are thought to be the debris left by comets which emitted them as dust tails in past years. Technically, they are known as meteoroids.

From the frequency with which comets appear in the solar system, Beard has estimated the rate at which dust is added to the solar system to be about 30 tons/sec. This rate of production may have continued for several billion years.

### THE POYNTING-ROBERTSON EFFECT

The dust particles in their solar orbits experience a continuous pressure from the solar radiation. The electromagnetic energy which they absorb is continuously reradiated isotropically. The exact analysis of this absorption and reemission shows that the dust particle experiences both an outward force away from the Sun, and a drag force tangential to the particle orbit. The drag force is a consequence of the fact that the momentum of the electromagnetic energy being radiated is greater than that being absorbed. The difference is made up at the expense of the particle's mechanical momentum. This effect was first described by Poynting and Robertson, and is named after them.

The effect of the radial force is to reduce the apparent attraction of the particle by the Sun. The effect of the drag force is to cause the particle to spiral inward in an orbit of continuously decreasing semimajor axis. Since the gravitational force depends on the particle volume and the radiation force depends on the particle cross-sectional area, the radiation effects become more and more important as the particle size diminishes. A particle 100 microns in diameter would spiral into the Sun in about 4000 years from the position of the Earth's orbit. A particle 1 centimeter in diameter would have a lifetime of $10^6$ to $10^7$ years. Before they reach the Sun, however, the particles will shrink from vaporization losses until the radiation pressure exceeds the Sun's gravitational attraction. At this point, the particles are quickly blown out of the solar system. The critical particle radius below which this loss takes place is about

$$a = 0.6/\rho \text{ micron}$$

where $\rho$ is the particle density. The Poynting-Robertson effect, then, clears away small particles in a very short time, and only bodies whose dimensions are of the order of meters can be as old as the solar system.

The gravitational attraction of the planets for the interplanetary dust is responsible for the concentration of dust in the ecliptic plane,

since cometary orbits do not show a statistical concentration in this plane. The attraction also causes many dust particles to become trapped in orbits around the planets, shrouding them in a blanket of dust whose numerical concentration is probably three orders of magnitude greater than that found in interplanetary space.

### EXPERIMENTAL MICROMETEOROID DETECTORS

The possible hazard to space flight which this blanket might represent, as well as the desire to verify the predictions made from various kinds of indirect evidence, has resulted in a large number of satellite experiments designed to measure the concentration of dust, and the momentum and mass distributions of the individual particles. The experiments have been designed chiefly to measure micrometeoroids, which are those particles which cannot be detected by optical or radar techniques. A reasonable upper limit to the size of these particles is about 1 millimeter.

The great majority of the measurements which have been made to date have utilized microphone or acoustical detectors. This detector consists of a metal plate to which is attached a piezoelectric crystal. The amplitude of the electrical signal which is generated when a micrometeoroid strikes the plate is a function of the mass and velocity of the particle, although the function is not easy to determine exactly. Detectors of this type can be made to respond to particles of momentum as low as $10^{-8}$ kg-m/sec.

The difficulties in interpretation of data from this type of detector are caused by sensitivity variations over the metal plate, by a lack of suitable laboratory sources of small high-speed particles, and by doubtful extrapolations and assumptions made from calibrations with the more easily available heavy particles traveling at low speeds.

Another type of detector is the impact light flash detector. This detector consists of a photomultiplier tube whose face is covered with a very thin layer of evaporated aluminum. A micrometeoroid which has sufficient energy to ionize itself or the target material on impact will produce a very brief ($<1$ $\mu$sec) light flash which is converted into an electrical signal by the photomultiplier tube. This detector shows promise of detecting particles whose mass is near the critical limit for loss by radiation pressure. Particles whose mass is $10^{-16}$ kilogram can be detected by this technique.

Another technique which appears to be of considerable interest for future experiments is the collection of ionization produced at the impact site. Experiments have shown that the charge collected is

$$Q = \frac{KE_pV}{A}$$

where $K$ is a constant of the target material, $E_p$ is the kinetic energy of the projectile, $V$ is the projectile velocity, and $A$ is the atomic weight of the projectile. This relationship has been shown to hold over three orders of magnitude of the collected charge.

In addition to the surface detectors described above, puncture detectors have been used to determine the penetration of micrometeoroids through selected thicknesses of different materials. One basic type of puncture detector is good for one event only. This type includes the pressurized-cell detector, the shielded-grid detector, and the wire-wound-insulator detector. The impact of a micrometeoroid in these detectors is recorded by the loss of gas pressure, by the change in electrical resistance when a grid wire is broken, and by the loss of electrical continuity when a wire is broken. Relating the mass and velocity of the particle to the damage which has been caused is, in every instance, based on rather crude theories and extrapolation from ground-based experiments. The loss of the detector after a single event is a further disadvantage.

Another type of puncture counter suffers cumulative damage as a thin layer of aluminum is eroded from a Mylar cover over a light-sensitive CdS cell. The damage is detected as a series of steps in electrical output which can be related to the size of the hole produced by the micrometeoroid.

A third type of detector is self-healing. An example of this type is a parallel-plate condenser consisting of evaporated metal layers on a very thin insulator of Mylar or MgO. Such a condenser discharges when penetrated by a micrometeoroid, and then appears to heal in the same way as an oil-filled capacitor after an internal discharge takes place.

One experiment has been performed on a recoverable sounding rocket to trap and return micrometeoroids. Some 133 particles thought to be of extraterrestrial origin were returned by this flight.

### THE RESULTS OF SATELLITE AND SPACE PROBE DUST MEASUREMENTS

The distribution of individual particle masses as measured by a number of satellite and sounding rocket experiments is shown in figure 5.1. Since many of the experiments measured momentum rather than mass, a velocity of 30 km/sec has been assumed to compute masses for all the data shown. The minimum mass which will not be blown away by radiation pressure is shown for several assumed particle densities. All of the experiments were performed rather close to the surface of the Earth, and the data represent a sampling of those particles which have been captured by the Earth.

Data from the Venus space probe Mariner II indicate, with large

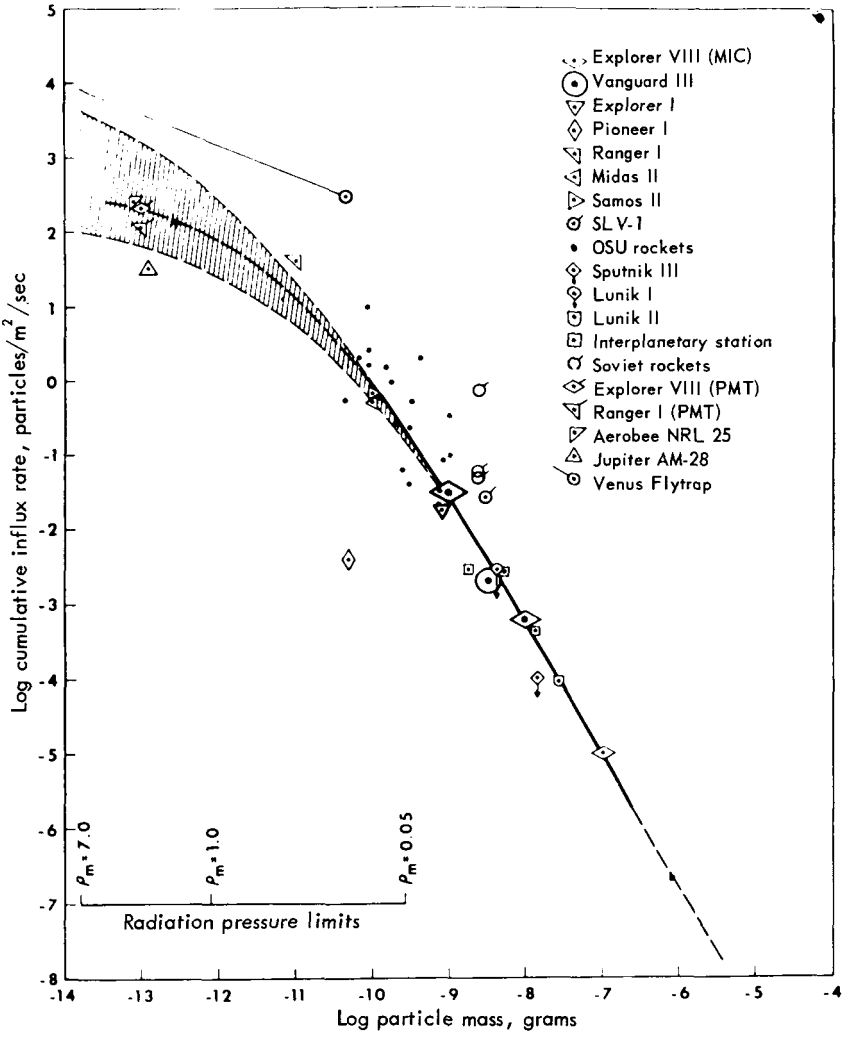


**FIGURE 5.1—Mass-distribution curve for micrometeorites, from microphone and photomultiplier data (ref. 1).**

statistical uncertainty, that the interplanetary flux of micrometeoroids is some four orders of magnitude lower than the flux near the Earth. This result is in reasonable agreement with the predictions of a dust blanket surrounding the Earth.

The experimental need in the field of micrometeoroid measurement is for techniques which measure both mass and velocity with reasonable accuracy over the wide range of these variables which is present. These techniques must provide sensitive surfaces of large area, par-

ticularly in interplanetary space where the fluxes are very low. Many of the difficulties which must be overcome exist because little laboratory work was done to develop appropriate instruments before space flights became available. The technology in the field is not nearly so advanced as the technology of nuclear particle instrumentation, for example. Much work is still required to produce suitable laboratory sources of artificial micrometeoroids for instrument calibration.

Considerable impetus to the solution of these problems has been given by the possible hazard to manned space flight which these particles may represent. This field can therefore be expected to develop rapidly in the future.

## REFERENCE

1. HAMERMESH, B.: Micrometeoroids. Space Physics, John Wiley & Sons, Inc., 1964, pp. 270–297.

# Bibliography


## CHAPTER 1

BEARD, D.: The Solar Wind-Geomagnetic Field Boundary. Rev. Geophys., vol. 2, 1964, pp. 335–365.

CAHILL, L. J., JR.: The Geomagnetic Field. Space Physics, D. P. LeGalley and A. Rosen, eds., John Wiley & Sons, Inc., 1964, pp. 301–349.

CHAPMAN, S.: Idealized Problems of Plasma Dynamics Relating to Geomagnetic Storms. Rev. Mod. Phys., vol. 32, 1962, pp. 919–933.

CHAPMAN, S.: Solar Plasma, Geomagnetism and Aurora. Geophysics, The Earth's Environment. Les Houches Lectures 1962. Gordon & Breach (New York), 1963, pp. 373–502.

CHAPMAN, S.; AND BARTELS, J.: Geomagnetism, Vols. I and II. Oxford, 1940.

HEPPNER, J. P.: The World Magnetic Survey. Space Sci. Rev., vol. 2, 1963, pp. 315–354.

RUDDOCK, K. A.: Optically Pumped Rubidium Vapor Magnetometer. Space Research II, H. C. van de Hulst, C. de Jager, and A. F. Moore, eds., North-Holland Pub. Co. (Amsterdam), 1961, pp. 692–700.

## CHAPTER 2

FARLEY, T. A.: The Growth of Our Knowledge of the Earth's Outer Radiation Belt. Rev. Geophys., vol. 1, 1963, pp. 3–34.

HESS, W. N.: Energetic Particles in the Inner Van Allen Belt. Space Sci. Rev., vol. 1, 1962–63, pp. 278–312.

LEGALLEY, D. P.; AND ROSEN, A., EDS.: Space Physics. John Wiley & Sons, Inc., 1964.

MCILWAIN, C. E.: Coordinates for Mapping the Distribution of Magnetically Trapped Particles. J. Geophys. Res., vol. 66, 1961, pp. 3681–3691.

NORTHROP, T. G.: The Adiabatic Motion of Charged Particles. Interscience Publishers, 1963.

O'BRIEN, B. J.: Review of Studies of Trapped Radiation With Satellite-Borne Apparatus. Space Sci. Rev., vol. 1, 1962–63, pp. 415–484.

## CHAPTER 3

BERNSTEIN, W.: The Solar Plasma—Its Detection, Measurement and Significance. Space Physics, D. P. LeGalley and A. Rosen, eds., John Wiley & Sons, Inc., 1964, pp. 397–436.

BIERMANN, L.: Solar Corpuscular Radiation and the Interplanetary Gas. Observatory, vol. 77, 1957, pp. 109–110.

CHAPMAN, S.: Notes on Solar Corona and Terrestrial Ionosphere. Smithsonian Contrib. Astrophys., vol. 2, 1957, pp. 1–14.

PARKER, E.: Interplanetary Dynamical Processes. Interscience Publishers, 1963.

SCARF, F.: The Solar Wind and Its Interaction With Magnetic Fields. Space Physics, D. P. LeGalley and A. Rosen, eds., John Wiley & Sons, Inc., 1964, pp. 437–473.

SMITH, E.: Interplanetary Magnetic Fields. Space Physics, D. P. LeGalley and A. Rosen, eds., John Wiley & Sons, Inc., 1964, pp. 350–396.

CHAPTER 4

ANDERSON, K. A.: Energetic Solar Particles. Space Physics, D. P. LeGalley and A. Rosen, eds., John Wiley & Sons, Inc., 1964, pp. 611–658.

BRYANT, D. A.; CLINE, T. L.; DESAI, U. D.; AND MCDONALD, F. B.: Studies of Solar Protons With Explorers XII and XIV. Astrophys. J., vol. 141, 1965, pp. 478–499.

KUIPER, G. P., ED.: The Sun. Univ. of Chicago Press (Chicago), 1953.

PARKER, E. N.: Interplanetary Dynamical Processes. Interscience Publishers, 1963.

ROSEN, A.; AND VOGL, J. L.: Cosmic Rays in Space. Space Physics, D. P. LeGalley and A. Rosen, eds., John Wiley & Sons, Inc., 1964, pp. 659–704.

SIMPSON, J. A.: Variations of Solar Origin in the Primary Cosmic Radiation. Astrophys. J. Suppl. Ser. IV, 1960, pp. 378–405.

CHAPTER 5

BEARD, D. B.: Comets and Cometary Debris in the Solar System. Rev. Geophys., vol. 1, 1963, pp. 211–229.

HAMERMESH, B.: Micrometeoroids. Space Physics, D. P. LeGalley and A. Rosen, eds., John Wiley & Sons, Inc., 1964, pp. 270–297.

ROBERTSON, H. P.: Dynamic Effects of Radiation in the Solar System. Monthly Notices of Roy. Astron. Soc., vol. 97, 1937, pp. 423–438.

The following articles are all contained in The Moon, Meteorites, and Comets. B. M. Middlehurst and G. P. Kuiper, eds., Univ. of Chicago Press (Chicago), 1963.

ROEMER, E.: Comets: Discovery, Orbits, Astrometric Observations. pp. 527–549.

PORTER, J. G.: The Statistics of Comet Orbits. pp. 550–572.

WURM, K.: The Physics of Comets. pp. 573–617.

BIERMANN, L.; AND LUST, R.: Comets: Structure and Dynamics of Tails. pp. 618–638.

WHIPPLE, F. L.: On the Structure of the Cometary Nucleus. pp. 639–664.

OORT, J. H.: Empirical Data on the Origin of Comets. pp. 665–673.

★U. S. GOVERNMENT PRINTING OFFICE: 1966—O 223-862